R. & M. No. 3673

R. & M. No. 3673

MINISTRY OF DEFENCE

AERONAUTICAL RESEARCH COUNCIL
REPORTS AND MEMORANDA

An Experimental Investigation of the Effect of Thickness on the Subsonic Longitudinal Stability Characteristics of Delta Wings of 70 Deg Sweep-Back

By D. A. KIRBY and D. L. I. KIRKPATRICK
Aerodynamics Dept., R.A.E., Farnborough

LONDON: HER MAJESTY'S STATIONERY OFFICE
1971
PRICE £1·50 NET

An Experimental Investigation of the Effect of Thickness on the Subsonic Longitudinal Stability Characteristics of Delta Wings of 70 Deg Sweep-Back

By D. A. KIRBY and D. L. I. KIRKPATRICK

Aerodynamics Dept., R.A.E., Farnborough

Reports and Memoranda No. 3673*
November, 1969

Summary.

Measurements of lift, drag and pitching moment have been made on five delta wing models to investigate the effects of thickness on the subsonic longitudinal characteristics of the 70 deg delta planform. For four of the wings the form of the thickness distribution was the same with the maximum thickness/chord ratios equal to 4, 8, 12 and 16 per cent respectively, but for the fifth wing a change in the type of thickness distribution was made whilst retaining the overall maximum thickness/chord ratio at 4 per cent.

The results showed that increase of thickness gave rise to losses in lift, reductions in lift-dependent drag and improvements in longitudinal stability.

LIST OF CONTENTS

Section

*Replaces R.A.E. Tech. Report No. 69256—A.R.C. 32 156.

---

1. *Introduction.*

In the investigation of the effect of planform shape on the subsonic longitudinal stability characteristics of slender wings reported in Ref. 1 the models tested were all comparatively thin and were all made with the same chordwise section in order to minimise the influence of thickness and thus facilitate identification of the important planform parameters. The maximum thickness/chord ratio of these models was 4 per cent, a value representative of the wing thickness of supersonic aircraft. Some effects of thickness were noted, but they were small and the second order interactions with the planform effects were considered to be very small.

There is however a possibility of using the slender-wing concept for the design of a subsonic airbus[2]. The attraction stems from the prospect of achieving an extremely compact layout—one in which the area the passenger cabin occupies is close to and entirely inside that of the wing. For such an all-wing aircraft the maximum thickness will be determined by the various cabin requirements, headroom etc. and, depending on the passenger capacity, the maximum thickness/chord ratio could range in size from, say, 15 per cent for 100 passengers to less than 10 per cent for 300 passengers.

With such large thickness/chord ratios the effects of thickness and of thickness distribution become significant[3]. Although considerable progress has been made in understanding the influence of cross-sectional shape on the normal force under conical flow conditions[4], there is at present no theoretical method available for determining the overall forces and moments for a thick slender wing in subsonic flow. In order to give an appreciation of the major effects of changes in thickness on the characteristics of a slender wing, a family of symmetrical delta wings of 70 deg sweep-back and with maximum thickness/chord ratios varying from 4 to 16 per cent has been tested, and the results are presented in this Report. The effects of camber in combination with thickness are currently being studied and will form the basis of a future report.

During the wind-tunnel tests a scale effect peculiar to the thick slender wing was discovered and this phenomenon is described in section 4. The effects of the various thickness distributions tested on lift and normal force are discussed in section 5.1 where the analysis is based, as in Ref. 1, on the assumption that the normal force can be split into linear and non-linear components arising from the attached and separated flow fields respectively. The changes in drag due to variations in thickness are considered in section 5.2 and finally in section 5.3 the pitching moments are analysed to find the aerodynamic-centre positions for the five wings.

2. *Details of Wings and Test Procedure.*

Each of the five wings tested was of delta planform with a leading-edge sweep-back angle, ϕ, of 70 deg and consequently an aspect ratio of 1·456 (Fig. 1). For four of the wings the thickness distribution was such that all the chordwise sections were of the same form. This distribution was specified by the equation.

$$t = \mathrm{T}(x-x_o)\left(1-\frac{x-x_o}{c_o-x_o}\right)\left(1-\tfrac{1}{2}\frac{x-x_o}{c_o-x_o}\right)$$

where t is the thickness of the wing at a point (x, y), $x_o = y \tan \phi$ and T is a constant governing the maximum thickness/chord ratio of the wing. All chordwise sections on each wing had the same maximum thickness/chord ratio and values of T were chosen so that the maximum thickness/chord ratios of the four wings were 4, 8, 12 and 16 per cent respectively. Fig. 1 shows the chordwise section shapes and Fig. 2 the spanwise cross-sections at 20, 40, 60 and 80 per cent of the centreline chord, c_o. The leading-edge angle of these spanwise cross-sections is constant for a particular wing and is given on both Figs. 1 and 2.

For the fifth wing the form of the thickness distribution was changed so that whilst the maximum thickness/chord ratio on the centreline remained at 4 per cent the edge angle of the spanwise cross-sections was increased to 59 deg, the value associated with the 8 per cent wing of the main series. This was done to provide preliminary data on the effect of 'flattening' the thickness distribution such as might be required for a practical all-wing aircraft. The form of the chordwise sections of the fifth wing varied across the span and only on the centreline was the maximum thickness/chord ratio equal to 4 per cent. For convenience this wing will be referred to in the Report as 4 per cent, 59 deg to distinguish it from the 4 per cent, 32 deg wing of the main series. The other wings will be designated by their thickness/chord ratios only.

All the wings were made of a resin-bonded glasscloth laminate sandwiched between two shaped teak fairings; the use of glasscloth allowed the leading edges to be better defined and less fragile than if teak had been used throughout.

The normal wire rig of the 4ft × 3ft wind-tunnel balance was used to support the wings and on each wing measurement of lift, drag and pitching moment were made with transition free, over an angle of incidence range from $\alpha = -5$ to 26 deg. For the 16 per cent only, some measurements were made with transition fixed following the discovery of separated flow over the rear part of the wing at low incidence —*see* section 4. The wind speed was generally 200 ft/sec, giving a Reynolds number based on the centreline chord of $2{\cdot}24 \times 10^6$. For the thickest wing, vibration prevented the use of this speed over the whole incidence range and some of the measurements were repeated at a speed of 100 ft/sec, with an extended incidence range following the discovery of irregularities in the development of the forces and moments with angle of incidence.

Some of the wings were later mounted on a sting support rig to obtain surface flow patterns. These were produced by painting the wing with a suspension of lampblack in kerosene, increasing the wind speed quickly to the desired value and keeping it constant while the suspension dried. The resulting pattern was then photographed and a selection of the photographs taken are presented in this Report.

3. *Calculation and Presentation of Results.*

The measured values of lift, drag and pitching moment were corrected for effects of wind-tunnel blockage and constraint. Although the models were nominally symmetrical, the results showed that some small asymmetries were present since for some of the wings a very small but finite lift and pitching moment were apparent at nominal zero incidence. Corrections for these distortions were made to the angle of incidence and pitching moment coefficient to ensure that zero lift and pitching moment occurred at zero incidence and the fully corrected coefficients are tabulated in Table 1. The largest value of $\Delta\alpha$ was 0·07 deg and the largest value of ΔC_m was 0·0008. Throughout the Report the pitching moment coefficients given are non-dimensionalized relative to the wing area and centreline chord and are referred to a moment centre at $0{\cdot}58\, c_o$.

The values of the lift, drag and pitching moment coefficients plotted against angle of incidence for all five wings are shown in Figs. 3–5, and the symbols used to designate the various wings in these figures are retained where possible throughout the Report.

4. *Scale Effect.*

In general the lift, drag and pitching moment curves show a smooth development with increase of

incidence of the type shown in Ref. 1. The discussion of scale effect in section 4 of that report is still relevant insomuch that, provided the leading edges are sharp, the development of the leading-edge vortices and consequently of the coefficients with increase of incidence is not materially affected by changes in Reynolds number. The results plotted in Figs. 3–5 for the 16 per cent wing of the present series show no appreciable effects resulting from the reduction in wind-tunnel speed from 200 ft/sec to 100 ft/sec at the high angles of incidence but at low incidence the values of lift and pitching moment were determined by the nature of the flow over the centre region of the wing rather than by the flow near the leading edge. Under transition free conditions the tests on the 16 per cent wing at 200 ft/sec showed that the lift slope reduced with increase of angle of incidence in the region of $\alpha = 2$ to 4 deg before subsequently following the normal pattern of development of non-linear lift associated with slender wings (Fig. 6).

The reason for this strange behaviour became apparent from the studies of the surface flow which showed that at low incidences the flow was laminar and separated from both wing surfaces aft of the maximum thickness line giving rise to weak swept vortices (Figs. 7–8). At small positive angles of incidence these vortices induced a positive lift increment and a nose-down pitching moment because on the lower surface, as the incidence increased, the extent and strength of the vortices decreased under the influence of the increasingly negative streamwise pressure gradient, whereas on the upper surface the vortices remained until the downwash from the leading-edge vortices was sufficiently strong to prevent separation on the rear part of the wing *cf* (Figs. 7 and 9a). At the higher Reynolds number this naturally occurred at a lower incidence—compare the extent of the separation on the lower surface in Figs. 7 and 8. Suppression of these separations at all incidences was achieved when turbulent flow over the whole wing was ensured by fixing grains of carborundum on both wing surfaces near the leading-edge (Fig. 9b). Initially the strips of roughness were about 0·5 inch wide, and close to the leading-edge, but the force and moment measurements showed that, in addition to removing the irregularities in the curves below $\alpha = 5$ deg, the lift of the wing at higher angles of incidence was also reduced (Fig. 10). This latter loss was shown by further tests to be due to excessive roughness interfering with the development of the leading-edge vortices and that roughness strips 0·1 inch wide fixed 0·1 inch inboard of the leading-edge were sufficient to suppress the separations aft of the maximum thickness line without affecting the lift at higher incidences (see Table 1 and Fig. 10).

5. *Discussion and Analysis of Results.*

5.1. *Lift and Normal Force.*

5.1.1. *Lift.* The curves of lift coefficient plotted against angle of incidence in Fig. 3 demonstrate one of the drawbacks of the all-wing aircraft. Design conditions such as ground clearance, cabin floor angle, undercarriage length etc. impose limitations on the usable incidence at take-off for all aircraft. For the present series of wings to achieve a typical take-off lift coefficient of 0·5 the thickest wing would need to be rotated about 2 deg further than the 4 per cent, 32 deg wing. The problem becomes less serious with increasing passenger capacity since for the same headroom the thickness/chord ratio can then be reduced; but the gains will depend very much on cross-section shape. For example, greater utilization of the plan area leads to larger edge angles and causes lift loses—compare the 4 per cent, 32 deg and 4 per cent, 59 deg wings in Fig. 3.

The reason for the kink in the lift coefficient curve of the 16 per cent wing at an angle of incidence of about 25 deg was not apparent from surface flow observations. Vibration of the model occurred at the attitude and it is possible that the kink results from a breakdown of the leading-edge vortices, but this is unlikely to be resolved without pressure plotting tests. No definite conclusions concerning the position of vortex breakdown on the 12 and 16 per cent wings were possible from the tests made by Earnshaw using the schlieren system[5].

5.1.2. *Normal force.* In studies of the influence of the various factors which control the lifting force on a slender wing it is more convenient from both theoretical and experimental standpoints to consider the flow relative to body rather than to wind axes. Therefore before proceeding with the analysis, the lift and drag coefficients have been used to calculate the normal force coefficient

$$C_N = C_L \cos\alpha + C_D \sin\alpha$$

and the axial force coefficient

$$C_A = -C_L \sin\alpha + C_D \cos\alpha$$

and these coefficients are included in Table 1.

The method of analysis then follows the principles adopted in Ref. 1, namely, that the flow past a slender wing with sharp edges can be considered as the sum of two velocity fields, the linear and the non-linear. The linear field is associated with the attached flow round the wing assumed to occur in slender body theory[6] and yields a lifting force which is directly proportional to the angle of incidence. The non-linear field is associated with the leading-edge vortices and generates a force which is a non-linear function of incidence. Hence the normal force coefficient is written as:—

$$C_N = C_{N_{\text{linear}}} + C_{N_{\text{non-linear}}} = a\alpha + C_{N_{\text{non-linear}}}$$

where a is the slope of the normal force characteristic at zero incidence.

For symmetrical sharp-edged wings where the leading-edge separation is established at all angles of incidence other than zero, the constant a in the equation should be determinable from plots of C_N/α against the angle of incidence, being for each wing the intercept of the curve with the C_N/α axis. Values of C_N/α are plotted for all five wings in Fig. 11. For the thinner wings C_N/α decreased monotonically towards $C_N/\alpha = a$ at zero incidence; but for the thicker wings the laminar separations, which occurred aft of the maximum thickness line and are discussed in section 4, caused spuriously large values of C_N/α, i.e. values which would not be attained on a full-scale aircraft. Although the tests with roughness added show that C_N/α under turbulent conditions would be smaller, it is evident that the addition of roughness has itself introduced some disturbance, and that the choice of values of a for the thicker wings must be to some extent speculative in the absence of tests at higher Reynolds numbers (Figs. 12 and 13). For all the wings the inaccuracy inherent in values of C_N/α at low angles of incidence must introduce uncertainty but ranges which should include the correct value of a for each wing were obtained from Figs. 12 and 13 and are shown in Fig. 14.

All the values are much less than the value of $a = \pi A/2$ which is predicted by slender body theory[6]. In a subsonic flow this would be expected because for the delta planform the theory fails to satisfy the Kutta-Joukowski condition of zero load at the trailing edge. In slender body theory the overall lifting force is dictated only by the spanwise cross-section at the trailing edge and, according to the theory for a family of wings of the type reported herein, as wing thickness is increased, an increase of the loading in the trailing-edge region should occur to balance a reduction of loading further forward. In reality the decrease of loading with increasing cross-section thickness does occur over the forward parts of the wing but the increase further back is not very marked because of the need to satisfy the Kutta condition (see Fig. 11 of Ref. 7).

Comparison of the possible values of a for the 4 per cent 32 deg wing with values obtained from other experiments on 4 per cent thick wings in the 4ft × 3ft tunnel showed that the lowest value of a was appropriate (Fig. 15), and this value has been assumed in drawing the mean curve for the family of wings in Fig. 14.

Values of a taken from the curve have then been used to obtain the non-linear component of the normal force, expressed as $C_N/\alpha - a$, associated with the separated or vortex flow field (Table 2). These values are plotted against the angle of incidence in Fig. 16 which shows that at incidences applicable to take-off and landing the non-linear component is not significantly affected by the wing thickness or by the thickness distribution. At very low angles of incidence there is evidence of some reduction in $C_N/\alpha - a$ with increasing thickness; this is in accordance with the results of tests under conical flow conditions[4].

5.2. *Drag and Axial Force.*

Except for the special exploration of the flow at low incidence on the 16 per cent wing described in section 4, free transition of the boundary layer from the laminar to the turbulent state was allowed. Under free transition conditions a far-aft transition occurred at very low angles of incidence and a laminar drag bucket was created (Fig. 17). This was naturally less marked on the thicker wings where the separations aft of the maximum thickness line were observed. To eliminate the effect of the low values of drag coefficient, C_{D_o}, at zero lift pertaining to the laminar drag bucket, new values of C_{D_o} have been obtained from extrapolation of the drag values at moderate incidences. These new values of C_{D_o}, plotted in Fig. 18 against the total frontal area, Φ, non-dimensionalized relative to the wing plan area, were used to calculate the values of the lift-dependent drag factor $K = (C_D - C_{D_o})/(C_L^2/\pi A)$ given in Table 1 and plotted in Fig. 19.

This figure shows that considerable decreases in the lift-dependent drag factor are obtained with increasing thickness. To determine the extent to which the beneficial effects of increased thickness can be applied to practical aircraft would of course require tests at both high and low speeds on correctly cambered models under trimmed conditions.

The reason for the reduction in lift-dependent drag with increasing thickness at moderate lift coefficients and the smaller changes which are measured at large lift coefficients becomes more apparent when the relationships

$$C_D = C_N \sin\alpha + C_A \cos\alpha\,,$$

$$C_L = C_N \cos\alpha - C_A \sin\alpha\,,$$

derived from the equations given in section 5.1.2, are used to rewrite the expression for K as follows:

$$K = \frac{\pi A}{C_L^2}(C_D - C_{D_o})$$

$$= \frac{\pi A}{C_L}\left(\frac{C_N \sin\alpha + C_A \cos\alpha - C_{D_o}}{C_N \cos\alpha - C_A \sin\alpha}\right)$$

$$= \frac{\pi A}{C_L}\left(\frac{\tan\alpha - (C_{D_o} - C_A)/C_N - C_{D_o}(\sec\alpha - 1)/C_N}{1 - C_A \tan\alpha / C_N}\right)$$

which since $C_A \tan\alpha / C_N << 1$ and $(1 - C_A/C_{D_o}) >> (\sec\alpha - 1)$ can be approximated as

$$K = \frac{\pi A}{C_L}\left(\tan\alpha - \frac{C_{D_o} - C_A}{C_N}\right).$$

For an infinitely thin wing K is entirely determined by the drag force ($= C_L \tan\alpha$) arising from the resolution of the normal force; but, for a thick slender wing the suctions induced by the leading-edge vortices on forward-facing surface produce a thrust component which reduces the axial force coefficient (Fig. 20). The size of this thrust component is a measure of the effectiveness of the planform and thickness distribution in creating forward-facing area on which the suctions beneath the leading-edge vortices can act and reduce the drag. Values of the thrust component, $C_{D_o} - C_A$, for all five wings are plotted in Fig. 21 against the corresponding non-linear components of the normal force. This figure shows not only the beneficial effects of an overall increase in thickness but also the advantages of concentrating increased thickness in the regions beneath the vortices—compare the results of the 4 per cent, 59 deg and the 4 per cent, 32 deg and 8 per cent wings. A close correlation with forward-facing area is demonstrated when the thrust component is referred to the frontal area rather than the wing area (Fig. 22).

The overall effect of thickness on the lift-dependent drag factor depends on the interplay between

the tan α and $(C_{D_o} - C_A)/C_N$ terms in the equation for K. At low and moderate angles of incidence and lift coefficient the reduction in $(C_A - C_{D_o})$ with thickness outweighs the concurrent increase in tan α resulting from the lower lift slope of the thicker wings (Fig. 3), but the advantage is almost lost at higher lift coefficients where the differences in tan α due to thickness changes increase rapidly.

5.3. *Pitching Moment and Longitudinal Stability.*

The pitching moment coefficients about a moment centre at 0·58 c_o are plotted against angle of incidence in Fig. 5 and lift coefficient in Fig. 23 for all five wings. At low angles of incidence the shape of the curves for the 12 per cent and 16 per cent wings is determined by the flow separations aft of the maximum thickness line, discussed in section 4, which occurred because of the low Reynolds number of the test. The special tests with roughness made to investigate the phenomenon showed that above $\alpha = 4$ deg the transition free results were reliable. Considering the transition fixed results of Fig. 10 in conjunction with the transition free results of Figs. 5 and 23 shows that following an initial destabilizing tendency at low angles of incidence, increases in wing thickness give increased longitudinal stability. For the wing of 16 per cent thickness/chord ratio this increase in longitudinal stability extended only to $\alpha = 22{\cdot}5$ deg, $C_L = 0{\cdot}8$, where the model vibration, probably due to vortex breakdown, occurred.

To assess the affects of thickness on the longitudinal stability it is necessary to determine the position of the aerodynamic centre since its position and development with increasing lift coefficient are of vital concern to the aircraft designer in fixing the empty aircraft's centre of gravity and the permissible variation in c.g. position with various fuel loads and payloads. The aerodynamic centre position has been calculated by measuring the slope $\partial C_m/\partial C_N$ at fixed values of lift coefficient and using the equation

$$\frac{dC_{m\ \text{aero centre}}}{d\alpha} = \frac{d}{d\alpha}\left(C_{m_{0\cdot 58}} - C_N \frac{\Delta hn}{c_o}\right) = 0 \text{ for neutral longitudinal stability}$$

where $C_{m\ \text{aero centre}}$ is the pitching moment coefficient relative to the aerodynamic centre

Δhn is the distance of the aerodynamic centre ahead of moment centre at 0·58 c_o.

The position expressed relative to the apex of each model is tabulated in Table 3 and plotted against lift coefficient in Fig. 24. The curves for the 4 per cent and 8 per cent wings can be defined accurately for most of the incidence range but the curves for the 12 and 16 per cent wings are to some extent speculative at low lift as is shown by the special plots of C_m v. C_N at low angles of incidence given in Fig. 25.

Above $C_L = 0{\cdot}3$ the effect of thickness on the aerodynamic centre position for a given lift coefficient is roughly constant. Increasing the thickness from 4 to 16 per cent causes a rearward movement of aerodynamic centre of about 5 per cent in the range of lift coefficient applicable to take-off and landing. Since movements of the aerodynamic centre rearwards are of benefit to the designer in the difficult act of balancing the slender-wing aircraft this effect of the increased thickness is very useful.

Because of the uncertainty concerning the values of C_m at low angles of incidence for the thicker wings, it is not possible to make a rigorous analysis of the contribution of the various linear and non-linear components to pitching moment. Tentatively it is assumed that the tests on the 16 per cent wing with transition fixed can be used to indicate the C_m v. C_N relationships of the 12 and 16 per cent wings at low angles of incidence. The point of action of the linear part of the normal force, i.e. that appropriate to attached flow, is given by the slope $\partial C_m/\partial C_N$ at $\alpha = 0$ and the dotted lines in Fig. 25 have been used to obtain the positions of the point of action for the five wings. These experimental positions relative to the wing apex are compared in Fig. 26a with positions calculated from slender-body theory by the method described in Appendix B of Ref. 1.

This figure confirms that the loss of lift in the experiment compared with the theoretical values which was noted in section 5.1.2 is concentrated towards the rear part of the wings; and that the thicker wings which according to the theory should carry comparatively more load near the trailing edge are more severely affected. This effect should be less marked for planforms with streamwise tips since the theory

then defines the loading more closely.

By subtraction of the linear component from the overall pitching moment and using the non-linear component of the normal force discussed earlier, the position of the point of action of the non-linear component can be calculated. In the tests on thin wings reported in Ref. 1, for all slender wing planforms this point of action moved forward with increasing incidence and for delta wings caused a pitch-up within the working range of lift coefficient. Increase of thickness has not changed this behaviour but there is an increase in longitudinal stability (Fig. 24) because at any given incidence the point of action of the non-linear component of the normal force is acting nearer the trailing edge (Fig. 26b).

6. *Concluding Remarks.*

Although the tests were confined to one delta planform the results presented in this Report demonstrate some of the major effects of wing thickness on the subsonic performance and longitudinal stability of slender wings in general.

The analysis assumes that the normal force and pitching moment on slender wings can be split into linear and non-linear components arising from the attached and separated flow fields respectively and considers the effects of increasing wing thickness on these two components. The results show that

(i) A reduction in overall lift occurs as wing thickness is increased because of a fall in the linear component of the normal force.

(ii) With increasing wing thickness the suction forces induced by the leading-edge vortices have an increasingly large forward component in the plane of the wing and consequently the lift-dependent drag of a thick slender wing is less than that of a thin wing with the same planform.

(iii) The point of action of the linear component of normal force moves forward with increasing thickness but that of the non-linear component moves rearward so that although the longitudinal stability is reduced with increasing thickness at low lift coefficients it is increased at lift coefficients appropriate to take-off and landing.

Further work is in progress to investigate the effect of thickness and camber on the characteristics of planforms with streamwise tips.

TABLE 1

Coefficients for the Five Wings.

α_{deg}	C_L	C_D	C_N	C_A	$C_{m_{0\cdot58}}$	C_N/α	K
4%, 32 deg		Transition free			V_o = 200 ft/sec		
−4·75	−0·1605	0·0170	−0·1614	0·0037	0·00398	1·947	
−4·24	−0·1414	0·0146	−0·1421	0·0041	0·00362	1·920	
−3·73	−0·1222	0·0124	−0·1227	0·0044	0·00331	1·890	
−3·19	−0·1036	0·0105	−0·1040	0·0047	0·00296	1·868	
−2·69	−0·0846	0·0090	−0·0850	0·0050	0·00266	1·811	
−2·18	−0·0677	0·0080	−0·0680	0·0054	0·00214	1·787	
−1·64	−0·0513	0·0071	−0·0515	0·0056	0·00178	1·799	
−1·15	−0·0358	0·0062	−0·0359	0·0055	0·00142	1·789	C_{D_o}=
−0·59	−0·0178	0·0047	−0·0178	0·0045	0·00031	1·729	
−0·15	−0·0046	0·0046	−0·0046	0·0046	0·00014	1·757	0·0057
+0·36	+0·0086	0·0046	+0·0086	0·0046	−0·00020	1·369	
0·87	0·0267	0·0058	0·0268	0·0054	−0·00138	1·765	
1·42	0·0420	0·0066	0·0422	0·0056	−0·00160	1·703	
1·95	0·0602	0·0073	0·0604	0·0053	−0·00205	1·755	
2·42	0·0745	0·0082	0·0748	0·0050	−0·00233	1·771	
2·96	0·0950	0·0095	0·0954	0·0046	−0·00286	1·847	1·926
3·47	0·1113	0·0110	0·1118	0·0043	−0·00306	1·846	1·957
3·99	0·1299	0·0131	0·1305	0·0041	−0·00340	1·874	2·006
4·50	0·1490	0·0154	0·1497	0·0037	−0·00376	1·906	1·999
5·02	0·1691	0·0183	0·1700	0·0034	−0·00402	1·940	2·015
5·59	0·1898	0·0213	0·1910	0·0027	−0·00435	1·958	1·981
6·57	0·2276	0·0280	0·2293	0·0018	−0·00487	2·000	1·969
7·61	0·2710	0·0372	0·2735	0·0009	−0·00523	2·059	1·962
8·64	0·3156	0·0481	0·3192	0·0002	−0·00548	2·117	1·947
9·68	0·3618	0·0611	0·3669	−0·0006	−0·00566	2·172	1·936
10·75	0·4089	0·0760	0·4159	−0·0009	−0·00574	2·217	1·923
11·71	0·4514	0·0912	0·4605	−0·0024	−0·00574	2·253	1·919
12·85	0·5032	0·1110	0·5152	−0·0037	−0·00583	2·297	1·902
13·84	0·5499	0·1309	0·5652	−0·0044	−0·00565	2·340	1·894
14·88	0·6012	0·1547	0·6208	−0·0049	−0·00494	2·391	1·886
15·92	0·6468	0·1775	0·6707	−0·0067	−0·00427	2·414	1·878
17·08	0·6994	0·2066	0·7292	−0·0080	−0·00320	2·446	1·879
18·06	0·7470	0·2339	0·7827	−0·0093	−0·00212	2·483	1·871
19·15	0·8008	0·2674	0·8442	−0·0011	−0·00115	2·526	1·867
20·14	0·8489	0·3002	0·9004	−0·0103	−0·00091	2·562	1·869
21·18	0·8973	0·3350	0·9577	−0·0119	+0·00182	2·591	1·870
22·23	0·9472	0·3715	1·0174	−0·0145	0·00345	2·622	1·865
23·22	0·9947	0·4109	1·0762	−0·0145	0·00500	2·656	1·873
24·26	1·0420	0·4523	1·1358	−0·0159	0·00678	2·683	1·881
25·30	1·0919	0·4970	1·1996	−0·0173	0·00917	2·717	1·885
26·34	1·1378	0·5422	1·2602	−0·0188	0·01086	2·741	1·896

TABLE 1 (Contd)

α_{deg}	C_L	C_D	C_N	C_A	$C_{m_{0.58}}$	C_N/α	K
4%, 59 deg			Transition free		V_o = 200 ft/sec		
−4·74	−0·1547	0·0157	−0·1555	0·0029	0·00396	1·879	
−4·22	−0·1317	0·0128	−0·1323	0·0031	0·00324	1·796	
−3·71	−0·1138	0·0111	−0·1143	0·0037	0·00270	1·765	
−3·19	−0·0956	0·0097	−0·0960	0·0044	0·00208	1·724	
−2·68	−0·0790	0·0087	−0·0793	0·0050	0·00155	1·695	
−2·16	−0·0632	0·0078	−0·0635	0·0054	0·00113	1·684	
−1·60	−0·0475	0·0071	−0·0477	0·0057	0·00062	1·708	
−1·14	−0·0353	0·0056	−0·0354	0·0049	0·00138	1·779	
−0·58	−0·0193	0·0053	−0·0194	0·0051	0·00072	1·916	C_{D_o} =
−0·11	−0·0021	0·0052	−0·0021	0·0052	0·00012	1·094	
+0·40	+0·0106	0·0052	+0·0106	0·0052	−0·00039	1·518	0·0061
0·91	0·0267	0·0054	0·0268	0·0051	−0·00040	1·681	
1·42	0·0400	0·0065	0·0401	0·0055	−0·00043	1·614	
1·94	0·0558	0·0074	0·0560	0·0055	−0·00105	1·650	
2·45	0·0721	0·0082	0·0724	0·0051	−0·00160	1·693	
2·96	0·0893	0·0091	0·0896	0·0041	−0·00220	1·734	1·778
3·48	0·1072	0·0103	0·1076	0·0038	−0·00274	1·772	1·711
4·00	0·1258	0·0121	0·1263	0·0033	−0·00329	1·810	1·763
4·56	0·1443	0·0143	0·1450	0·0028	−0·00380	1·822	1·823
5·03	0·1638	0·0168	0·1646	0·0024	−0·00414	1·875	1·841
5·54	0·1808	0·0196	0·1817	0·0012	−0·00449	1·879	1·903
6·57	0·2198	0·0260	0·2213	0·0007	−0·00125	1·930	1·894
7·61	0·2625	0·0346	0·2648	−0·0005	−0·00616	1·994	1·899
8·65	0·3066	0·0452	0·3099	−0·0014	−0·00632	2·053	1·907
9·73	0·3514	0·0574	0·3561	−0·0028	−0·00665	2·097	1·903
10·72	0·3967	0·0716	0·4031	−0·0034	−0·00664	2·155	1·907
11·76	0·4382	0·0859	0·4465	−0·0052	−0·00647	2·176	1·903
12·85	0·4863	0·1044	0·4973	−0·0064	−0·00636	2·218	1·903
13·89	0·5377	0·1257	0·5522	−0·0070	−0·00644	2·280	1·894
14·88	0·5844	0·1467	0·6025	−0·0083	−0·00642	2·320	1·884
15·92	0·6313	0·1697	0·6537	−0·0099	−0·00638	2·353	1·879
16·96	0·6838	0·1975	0·7117	−0·0107	−0·00587	2·405	1·873
18·00	0·7282	0·2233	0·7616	−0·0126	−0·00522	2·424	1·875
18·99	0·7730	0·2508	0·8126	−0·0143	−0·00395	2·452	1·874
20·13	0·8270	0·2868	0·8752	−0·0154	−0·00247	2·491	1·878
21·17	0·8753	0·3212	0·9322	−0·0165	−0·00019	2·523	1·882
22·16	0·9185	0·3530	0·9838	−0·0195	0·00078	2·544	1·882
23·31	0·9731	0·3962	1·0505	−0·0213	0·00199	2·582	1·885
24·24	1·0166	0·4323	1·1044	−0·0231	0·00290	2·611	1·886
25·28	1·0615	0·4729	1·1618	−0·0256	0·00451	2·633	1·895
26·38	1·1137	0·5228	1·2300	−0·0313	0·00599	2·672	1·905

TABLE 1 (Contd)

α_{deg}	C_L	C_D	C_N	C_A	$C_{m_{0\cdot58}}$	C_N/α	K
8%			Transition free			V_o = 200 ft/sec	
−4·68	−0·1459	0·0153	−0·1467	0·0034	0·00460	1·796	
−4·17	−0·1322	0·0139	−0·1329	0·0042	0·00425	1·826	
−3·66	−0·1142	0·0123	−0·1148	0·0050	0·00346	1·797	
−3·14	−0·0917	0·0106	−0·0921	0·0055	0·00233	1·681	
−2·62	−0·0752	0·0097	−0·0756	0·0063	0·00161	1·653	
−2·11	−0·0587	0·0078	−0·0590	0·0066	0·00102	1·602	
−1·60	−0·0430	0·0078	−0·0432	0·0066	0·00063	1·547	
−1·09	−0·0300	0·0064	−0·0301	0·0058	0·00095	1·582	
−0·57	−0·0174	0·0063	−0·0175	0·0061	0·00061	1·759	C_{D_o} =
−0·06	−0·0011	0·0062	−0·0011	0·0062	0·00001	1·051	
+0·45	+0·0135	0·0062	+0·0136	0·0061	−0·00036	1·719	0·0070
0·97	0·0315	0·0064	0·0316	0·0059	−0·00059	1·867	
1·50	0·0425	0·0076	0·0427	0·0065	−0·00069	1·623	
1·99	0·0550	0·0084	0·0553	0·0065	−0·00090	1·592	
2·52	0·0710	0·0093	0·0713	0·0062	−0·00150	1·614	
3·01	0·0278	0·0100	0·0883	0·0053	−0·00213	1·681	1·780
3·56	0·1060	0·0113	0·1065	0·0047	−0·00288	1·714	1·750
4·04	0·1239	0·0127	0·1245	0·0040	−0·00351	1·766	1·698
4·56	0·1404	0·0146	0·1411	0·0034	−0·00406	1·764	1·764
5·08	0·1618	0·0170	0·1627	0·0026	−0·00477	1·835	1·747
5·59	0·1787	0·0195	0·1798	0·0020	−0·00527	1·832	1·790
6·67	0·2167	0·0257	0·2182	0·0003	−0·00638	1·874	1·822
7·66	0·2575	0·0334	0·2563	−0·0012	−0·00727	1·917	1·821
8·69	0·2942	0·0417	0·2971	−0·0032	−0·00818	1·959	1·834
9·67	0·3368	0·0525	0·3408	−0·0047	−0·00900	2·019	1·835
10·66	0·3810	0·0653	0·3865	−0·0063	−0·00975	2·078	1·837
11·80	0·4273	0·0805	0·4347	−0·0086	−0·01024	2·111	1·841
12·89	0·4750	0·0975	0·4848	−0·0109	−0·01058	2·155	1·835
13·88	0·5218	0·1162	0·5344	−0·0123	−0·01107	2·206	1·835
15·02	0·5711	0·1378	0·5873	−0·0150	−0·01113	2·240	1·835
15·95	0·6132	0·1580	0·6329	−0·0166	−0·01093	2·274	1·837
17·00	0·6634	0·1837	0·6881	−0·0183	−0·01113	2·319	1·836
18·04	0·7112	0·2102	0·7413	−0·0203	−0·01127	2·355	1·838
19·13	0·7616	0·2400	0·7982	−0·0229	−0·01052	2·391	1·838
20·12	0·8066	0·2696	0·8501	−0·0244	−0·00972	2·421	1·846
21·21	0·8577	0·3048	0·9095	−0·0262	−0·00875	2·457	1·852
22·25	0·9050	0·3391	0·9660	−0·0288	−0·00833	2·488	1·855
23·24	0·9508	0·3744	1·0214	−0·0312	−0·00743	2·518	1·859
24·28	0·9960	0·4127	1·0778	−0·0334	−0·00654	2·544	1·871
25·32	1·0453	0·4536	1·1389	−0·0371	−0·00554	2·577	1·870
26·36	1·0926	0·4972	1·1998	−0·0396	−0·00510	2·608	1·878

TABLE 1 (Contd)

α_{deg}	C_L	C_D	C	C_A	$C_{m_{0.58}}$	C_N/α	K
12%			Transition free			V_o = 200 ft/sec	
−3·79	−0·1033	0·0122	−0·1039	0·0053	0·00151	1·571	
−3·23	−0·0891	0·0110	−0·0896	0·0059	0·00126	1·570	
−2·76	−0·0759	0·0101	−0·0763	0·0065	0·00108	1·584	
−2·25	−0·0647	0·0089	−0·0650	0·0063	0·00180	1·655	
−1·74	−0·0518	0·0080	−0·0520	0·0064	0·00199	1·712	
−1·23	−0·03 8	0·0077	−0·0360	0·0069	0·00125	1·677	
−0·72	−0·0202	0·0075	−0·0203	0·0072	0·00065	1·623	C_{D_o} =
−0·20	−0·0048	0·0074	−0·0048	0·0074	0·00003	1·375	
+0·32	+0·0086	0·0073	+0·0086	0·0073	−0·00036	1·540	0·0079
0·82	0·0255	0·0075	0·0256	0·0071	−0·00099	1·788	
1·29	0·0378	0·0077	0·0380	0·0068	−0·00138	1·688	
1·79	0·0537	0·0081	0·0539	0·0064	−0·00209	1·725	
2·34	0·0683	0·0085	0·0686	0·0056	−0·00245	1·680	
2·87	0·0787	0·0103	0·0791	0·0064	−0·00121	1·579	
3·37	0·0892	0·0110	0·0897	0·0058	−0·00123	1·525	1·782
3·89	0·1037	0·0119	0·1043	0·0049	−0·00131	1·536	1·701
4·40	0·1174	0·0130	0·1180	0·0040	−0·00172	1·537	1·693
4·91	0·1352	0·0143	0·1359	0·0027	−0·00214	1·586	1·602
5·43	0·1528	0·0162	0·1536	0·0017	−0·00321	1·621	1·626
6·46	0·1883	0·8205	0·1894	−0·0008	−0·00486	1·680	1·625
7·51	0·2268	0·0264	0·2283	−0·0035	−0·00711	1·742	1·645
8·52	0·2663	0·0343	0·2684	−0·0055	−0·00911	1·805	1·703
9·56	0·3058	0·0433	0·3087	−0·0082	−0·01074	1·850	1·731
10·59	0·3472	0·0539	0·3512	−0·0108	−0·01265	1·900	1·745
11·63	0·3907	0·0667	0·3961	−0·0135	−0·01456	1·951	1·762
12·66	0·4339	0·0805	0·4410	−0·0166	−0·01614	1·996	1·764
13·75	0·4786	0·0966	0·4878	−0·0200	−0·01767	2·033	1·771
14·73	0·5184	0·1121	0·5298	−0·0235	−0·01848	2·061	1·774
15·77	0·5632	0·1313	0·5777	−0·0267	−0·01959	2·099	1·779
16·84	0·6075	0·1525	0·6256	−0·0299	−0·02032	2·129	1·792
17·90	0·6535	0·1759	0·6759	−0·0335	−0·02087	2·163	1·799
18·88	0·6947	0·1986	0·7216	−0·0369	−0·02127	2·190	1·807
19·92	0·7410	0·2250	0·7737	−0·0400	−0·02193	2·225	1·817
21·01	0·7877	0·2561	0·8271	−0·0439	−0·02209	2·256	1·829
22·00	0·8293	0·2841	0·8753	−0·0472	0·02241	2·280	1·837
23·04	0·8769	0·3183	0·9315	−0·0501	−0·02306	2·316	1·846
24·07	0·9199	0·3515	0·9833	−0·0542	−0·02324	2·341	1·858
25·11	0·9638	0·3868	1·0368	−0·0589	−0·02334	2·366	1·866
26·15	1·0081	0·4262	1·0927	−0·0617	−0·02350	2·394	1·883

TABLE 1 (Contd)

α_{deg}	C_L	C_D	C_N	C_A	$C_{m_{0\cdot58}}$	C_N/α	K
16%			Transition free			V_o = 200 ft/sec	
−4·68	−0·1139	0·0144	−0·1147	0·0051	−0·00068	1·404	
−4·16	−0·1000	0·0134	−0·1007	0·0061	−0·00085	1·387	
−3·65	−0·0879	0·0124	−0·0885	0·0068	−0·00071	1·389	
−3·15	−0·0782	0·0114	−0·0787	0·0072	0	1·432	
−2·64	−0·0696	0·0103	−0·0700	0·0071	+0·00119	1·519	
−2·13	−0·0620	0·0093	−0·0624	0·0070	0·00243	1·679	
−1·62	−0·0470	0·0089	−0·0472	0·0076	0·00181	1·669	
−1·11	−0·0323	0·0086	−0·0325	0·0080	0·00123	1·678	
−0·60	−0·0172	0·0084	−0·0173	0·0082	0·00068	1·652	C_{D_o}=
−0·17	−0·0032	0·0083	−0·0032	0·0083	−0·00001	1·079	
+0·43	+0·0120	0·0082	+0·0120	0·0081	−0·00060	1·612	0·0091
0·89	0·0267	0·0084	0·0268	0·0080	−0·00114	1·725	
1·44	0·0420	0·0086	0·0422	0·0076	−0·00171	1·679	
1·97	0·0569	0·0089	0·0572	0·0070	−0·00213	1·664	
2·46	0·0667	0·0098	0·0671	0·0069	−0·00140	1·563	
2·98	0·0753	0·0107	0·0758	0·0068	−0·00042	1·457	
3·49	0·0836	0·0117	0·0842	0·0066	+0·00069	1·382	
4·00	0·0954	0·0125	0·0960	0·0058	0·00082	1·375	1·709
4·51	0·1089	0·0124	0·1096	0·0048	0·00080	1·392	1·659
5·02	0·1229	0·0146	0·1237	0·0038	0·00048	1·412	1·666
5·49	0·1370	0·0158	0·1379	0·0026	0·00014	1·439	1·632
6·56	0·1721	0·0194	0·1732	−0·0004	−0·00122	1·513	1·591
7·59	0·2057	0·0239	0·2071	−0·0035	−0·00266	1·563	1·600
8·62	0·2426	0·0298	0·2468	−0·0070	−0·00520	1·641	1·610
9·66	0·2813	0·0372	0·2836	−0·0106	−0·00762	1·682	1·624
10·69	0·3197	0·0458	0·3226	−0·0143	−0·01006	1·729	1·642
11·67	0·3603	0·0563	0·3642	−0·0174	−0·01269	1·788	1·663
12·76	0·4057	0·0698	0·4110	−0·0216	−0·01563	1·846	1·687
13·79	0·4472	0·0836	0·4542	−0·0253	−0·01799	1·887	1·706
14·83	0·4885	0·0992	0·4976	−0·0291	−0·01985	1·923	1·728
15·87	0·5316	0·1164	0·5432	−0·0334	−0·02203	1·916	1·737
16·90	0·5750	0·1349	0·5894	−0·0381	−0·02412	1·998	1·740
17·94	0·6175	0·1551	0·6352	−0·0426	−0·02552	2·029	1·751
18·94	0·6569	0·1756	0·6780	−0·0461	−0·02734	2·051	1·765
20·01	0·6980	0·1990	0·7240	−0·0519	−0·02855	2·073	1·783
21·04	0·7413	0·2256	0·7728	−0·0555	−0·02965	2·105	1·802
22·07	0·7793	0·2504	0·8163	−0·0607	−0·03014	2·119	1·817
23·16	0·8175	0·2781	0·8610	−0·0659	−0·02993	2·129	1·841
24·17	0·8413	0·2981	0·8896	−0·0724	−0·02546	2·109	1·868

TABLE 1 (Contd)

α_{deg}	C_L	C_D	C_N	C_A	$C_{m_{0.58}}$	C_N/α	K
16%			Transition free			V_o = 100 ft/sec	
−4·52	−0·1167	0·0154	−0·1176	0·0062	0·00207	1·491	
−3·50	−0·0960	0·0131	−0·0966	0·0072	0·00288	1·581	
−2·48	−0·0719	0·0117	−0·0723	0·0086	0·00280	1·670	
−1·97	−0·0577	0·0115	−0·0581	0·0095	0·00229	1·690	
−1·46	−0·0423	0·0105	−0·0426	0·0094	0·00138	1·672	
−0·94	−0·0274	0·0103	−0·0276	0·0098	0·00078	1·682	
−0·43	−0·0133	0·0100	−0·0134	0·0099	−0·00018	1·786	
+0·07	−0·0064	0·0100	−0·0064	0·0100	+0·00011	−0·524	
0·59	+0·0159	0·0100	+0·0159	0·0098	−0·00070	1·544	
1·11	0·0314	0·0103	0·0316	0·0097	−0·00131	1·631	
1·62	0·0482	0·0105	0·0485	0·0091	−0·00185	1·715	
2·13	0·0609	0·0110	0·0613	0·0087	−0·00220	1·649	
2·64	0·0759	0·0119	0·0764	0·0084	−0·00296	1·658	
3·15	0·0893	0·0127	0·0899	0·0077	−0·00283	1·635	
3·66	0·0992	0·0132	0·0998	0·0068	−0·00062	1·562	
4·68	0·1192	0·0155	0·1205	0·0057	−0·00091	1·475	
5·70	0·1487	0·0182	0·1498	0·0033	−0·00174	1·506	
6·73	0·1791	0·0218	0·1804	0·0006	−0·00275	1·536	
7·76	0·2119	0·0265	0·2135	−0·0023	−0·00394	1·576	
8·81	0·2482	0·0327	0·2503	−0·0057	−0·00567	1·628	
9·82	0·2876	0·0404	0·2903	−0·0092	−0·00833	1·694	
10·80	0·3285	0·0496	0·3319	−0·0128	−0·01133	1·761	
11·78	0·3667	0·0588	0·3710	−0·0177	−0·01170	1·805	
12·76	0·4074	0·0712	0·4130	−0·0206	−0·01515	1·855	
13·80	0·4481	0·0848	0·4553	−0·0246	−0·01675	1·890	C_{D_o} =
14·83	0·4931	0·1005	0·5024	−0·0290	−0·01935	1·941	
15·86	0·5302	0·1158	0·5417	−0·0336	−0·02177	1·957	0·0106
16·90	0·5744	0·1356	0·5890	−0·0373	−0·02343	1·997	
17·94	0·6167	0·1555	0·6346	−0·0419	−0·02547	2·027	
19·03	0·6640	0·1784	0·6859	−0·0479	−0·02825	2·065	1·741
20·11	0·7071	0·2033	0·7339	−0·0523	−0·02965	2·091	1·763
21·10	0·7461	0·2276	0·7780	−0·0562	−0·03067	2·113	1·780
22·08	0·7857	0·2521	0·8228	−0·0617	−0·03053	2·135	1·798
23·11	0·8176	0·2761	0·8603	−0·0671	−0·03034	2·133	1·817
24·12	0·8327	0·2988	0·8821	−0·0675	−0·02697	2·096	1·901
25·19	0·8620	0·3280	0·9196	−0·699	−0·02520	2·092	1·954
26·16	0·8811	0·3530	0·9465	−0·0717	−0·02203	2·073	2·017
27·23	0·9063	0·3840	0·9816	−0·0733	−0·02140	2·066	2·079
28·27	0·9530	0·4255	1·0408	−0·0765	−0·02495	2·110	2·107
29·26	0·9963	0·4660	1·0968	−0·0805	−0·02719	2·1 8	2·099
30·29	1·0388	0·5076	1·1530	−0·0854	−0·02907	2·181	2·107
31·33	1·0779	0·5492	1·2063	−0·0914	−0·02955	2·206	2·120
32·36	1·1167	0·5918	1·2600	−0·0979	−0·03126	2·231	2·132
33·40	1·1570	0·6420	1·3193	−0·1009	−0·03324	2·263	2·157
34·43	1·1914	0·6883	1·3718	−0·1046	−0·03424	2·282	2·184
35·45	1·2242	0·7345	1·4232	−0·1117	−0·03511	2·300	2·209
36·48	1·2549	0·7841	1·4752	−0·1157	−0·03553	2·316	2·247

TABLE 1 (Contd)

α_{deg}	C_L	C_D	C_N	C_A	$C_{m_{0.58}}$	C_N/α	K
16%			Transition fixed by roughness band 0·5 in wide parallel to leading-edge			V_o = 200 ft/sec	
−4·73	−0·1160	0·0190	−0·1172	0·0094	−0·00095	1·420	
−3·66	−0·0907	0·0173	−0·0916	0·0115	−0·00074	1·434	
−2·64	−0·0663	0·0160	−0·0670	0·0129	−0·00041	1·454	
−1·61	−0·0414	0·0151	−0·0418	0·0139	−0·00029	1·488	C_{D_o} =
−0·59	−0·0162	0·0146	−0·0163	0·0144	−0·00018	1·583	
+0·41	+0·0121	0·0145	+0·0122	0·0144	+0·00002	1·733	0·0145
1·45	0·0365	0·0148	0·0369	0·0138	0·00011	1·458	
2·42	0·0601	0·0154	0·0607	0·0129	0·00054	1·437	
3·49	0·0852	0·0165	0·0860	0·0112	0·00065	1·412	1·260
4·46	0·1092	0·0180	0·1102	0·0094	0·00091	1·416	1·343
5·48	0·1338	0·0202	0·1351	0·0073	0·00095	1·413	1·457
6·56	0·1635	0·0234	0·1651	0·0046	0·00052	1·442	1·523
7·58	0·1927	0·0272	0·1946	0·0015	−0·00042	1·471	1·564
8·61	0·2267	0·0321	0·2290	−0·0022	−0·00209	1·524	1·566
9·64	0·2627	0·0385	0·2654	−0·0060	−0·00405	1·578	1·591
10·67	0·3011	0·0470	0·3046	−0·0095	−0·00643	1·636	1·640
15·80	0·5114	0·1141	0·5231	−0·0294	−0·01940	1·897	1·742
20·98	0·7300	0·2238	0·7617	−0·0524	−0·02619	2·080	1·796
			Transition fixed by roughness band 0·1 in wide parallel to leading-edge			V_o = 200 ft/sec	
−4·72	−0·1110	0·0168	−0·1120	0·0076	−0·00065	1·360	C_{D_o} =
0·38	+0·0128	0·0126	+0·0129	0·0125	−0·00024	1·945	0·0126
5·49	0·1406	0·0182	0·1417	0·0046	−0·00023	1·479	1·296
10·64	0·3178	0·0462	0·3209	−0·0132	−0·00922	1·728	0·522
15·81	0·5236	0·1143	0·5350	−0·0327	−0·02127	1·939	1·696
21·00	0·7469	0·2271	0·7787	−0·0556	−0·03160	2·125	1·759

TABLE 2

Linear and Non-Linear Normal Force Components

	α^o	4%, 32 deg	4%, 59 deg	8%	12%	16%
Linear a		1·65	1·57	1·50	1·34	1·17
Non-linear						
	2	0·12	0·11	0·10	0·09	0·08
	4	0·23	0·23	0·22	0·20	0·18
	6	0·34	0·33	0·34	0·32	0·30
$C_N/\alpha - a$	8	0·43	0·44	0·44	0·43	0·42
	12	0·61	0·63	0·62	0·61	0·63
	16	0·77	0·78	0·78	0·76	0·80
	20	0·90	0·91	0·92	0·88	0·91
	24	1·03	1·03	1·04	1·00	

TABLE 3

Distance of Aerodynamic Centre Aft of Wing Apex

C_L	4%, 32 deg	4%, 59 deg	8%	12%	16%
0	0·610	0·594	0·596	0·587	0·572
0·1	0·600	0·609	0·620	0·602	0·581
0·2	0·593	0·599	0·608	0·632	0·628
0·3	0·587	0·588	0·599	0·626	0·643
0·4	0·582	0·580	0·592	0·614	0·639
0·5	0·576	0·578	0·586	0·605	0·626
0·6	0·569	0·575	0·580	0·596	0·616
0·7	0·563	0·568	0·574	0·590	0·608
0·8	0·558	0·558	0·569	0·587	
0·9	0·543	0·545	0·566	0·584	

LIST OF REFERENCES

No.	*Author(s)*	*Title, etc.*
1	D. A. Kirby	An experimental investigation of the effect of planform shape on the subsonic longitudinal stability characteristics of slender wings. A.R.C. R. & M. 3568 (1967).
2	D. Kuchemann and J. Weber	An analysis of some performance aspects of various types of aircraft designed to fly over different ranges at different speeds. Prog. in Aero. Sci., 9, 1968 pp. 329–456 R.A.E. Technical Report 66188 A.R.C. 28369 (1966).
3	D. H. Peckham	Low-speed wind-tunnel tests on a series of uncambered slender pointed wings with sharp edges. A.R.C. R. & M. 3186 (1958).
4	D. L. I. Kirkpatrick	Investigation of the normal force characteristics of slender delta wings with various rhombic cross-sections in subsonic conical flow. A.R.C. CP 922 (1965).
5	P. B. Earnshaw	Measurements of the effects of thickness on vortex breakdown position on a series of sharp-edged delta wings. A.R.C. CP 1018 (1968).
6	Robert T. Jones	Properties of low aspect ratio pointed wings at speeds below and above the speed of sound. NACA TN 1032 (A.R.C. 9483) (1946).
7	D. L. I. Kirkpatrick	Analysis of the static pressure distribution on a delta wing in subsonic flow. A.R.C. R. & M. 3619 (1968).
8	D. A. Kirby	Low-speed wind-tunnel measurements of the lift, drag and pitching moment of a series of cropped-delta wings. R.A.E. Report to be published.

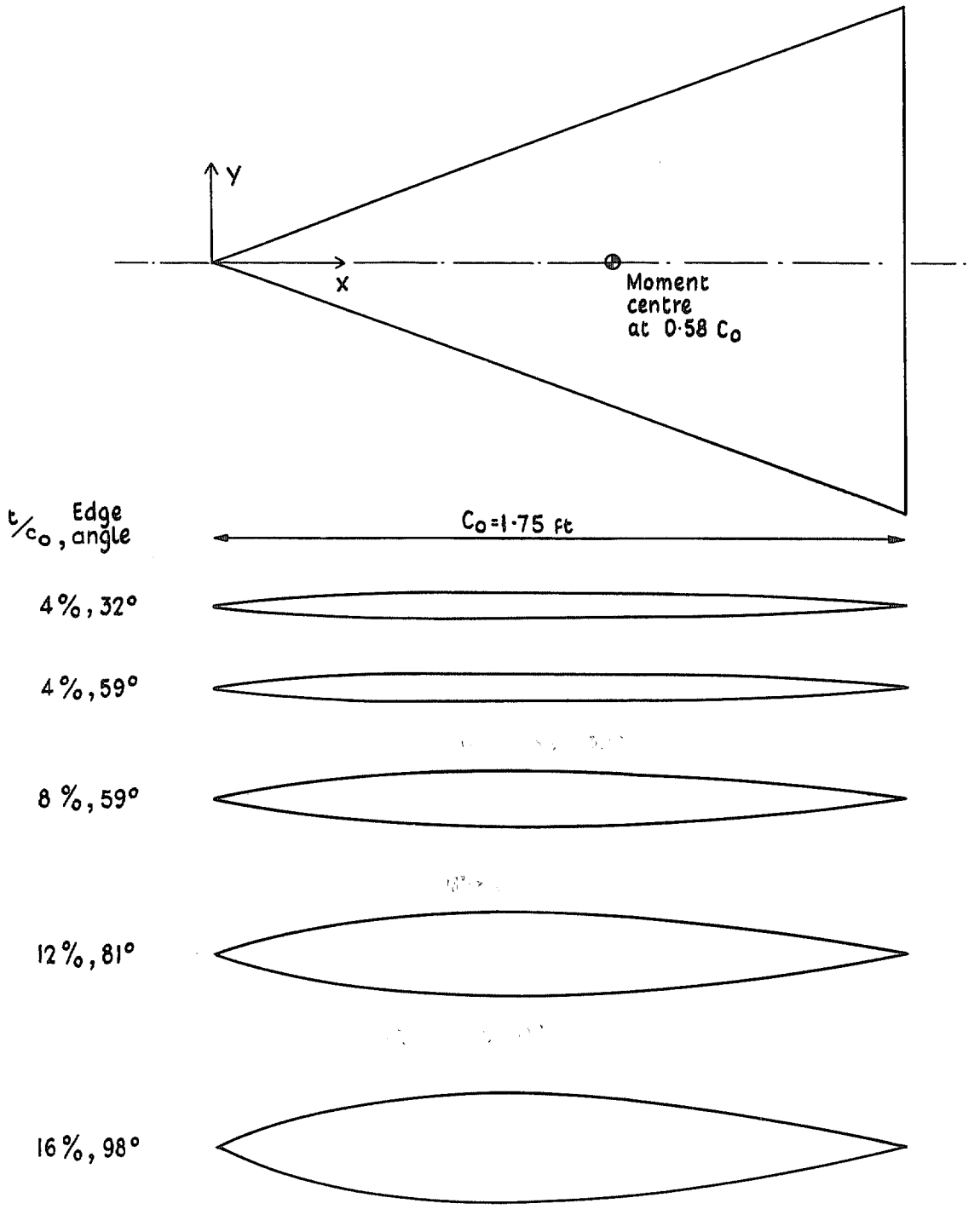

FIG. 1. Planform and centre line sections.

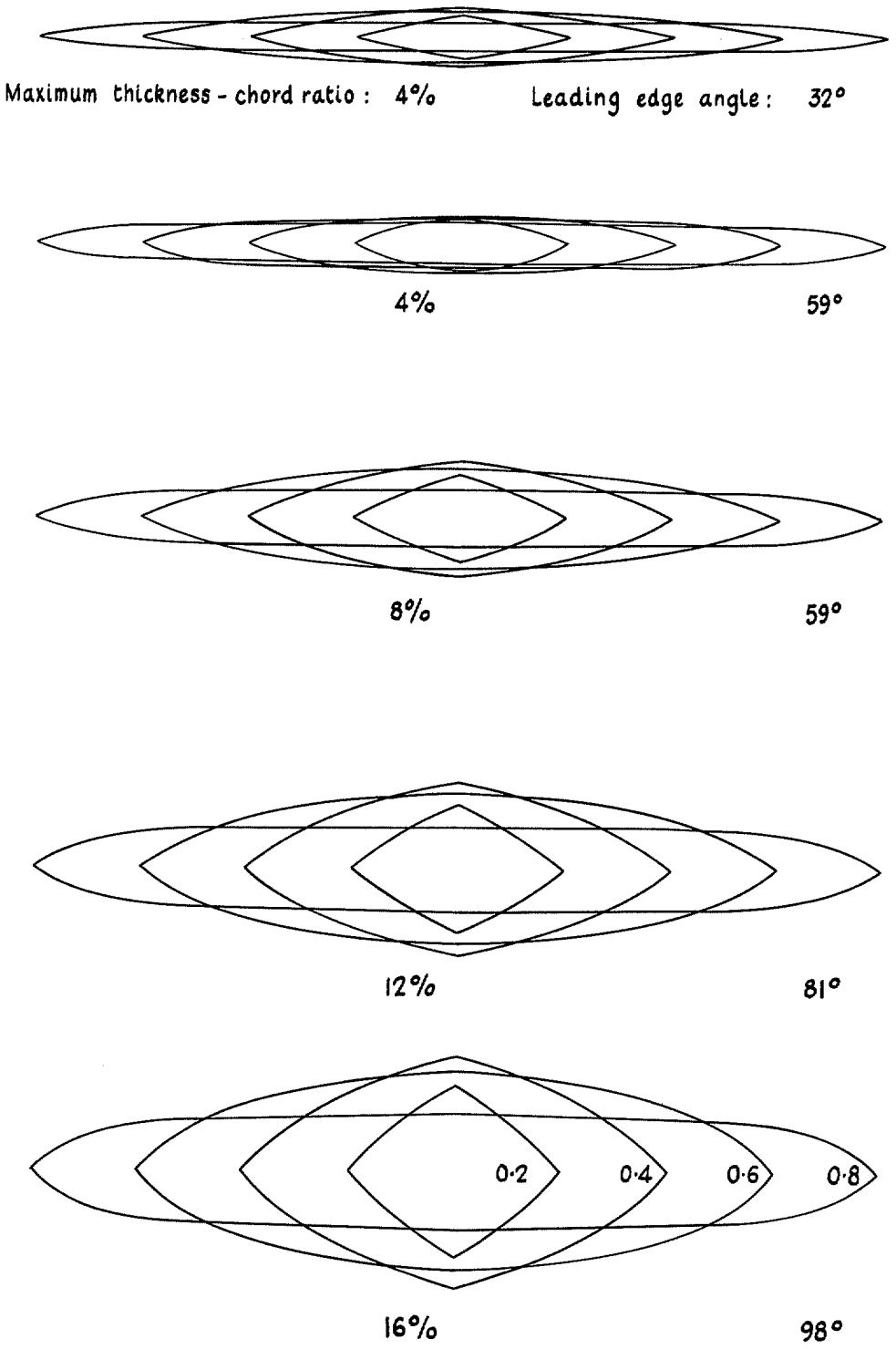

FIG. 2. Spanwise cross sections at 0·2, 0·4, 0·6 and 0·8 c_o.

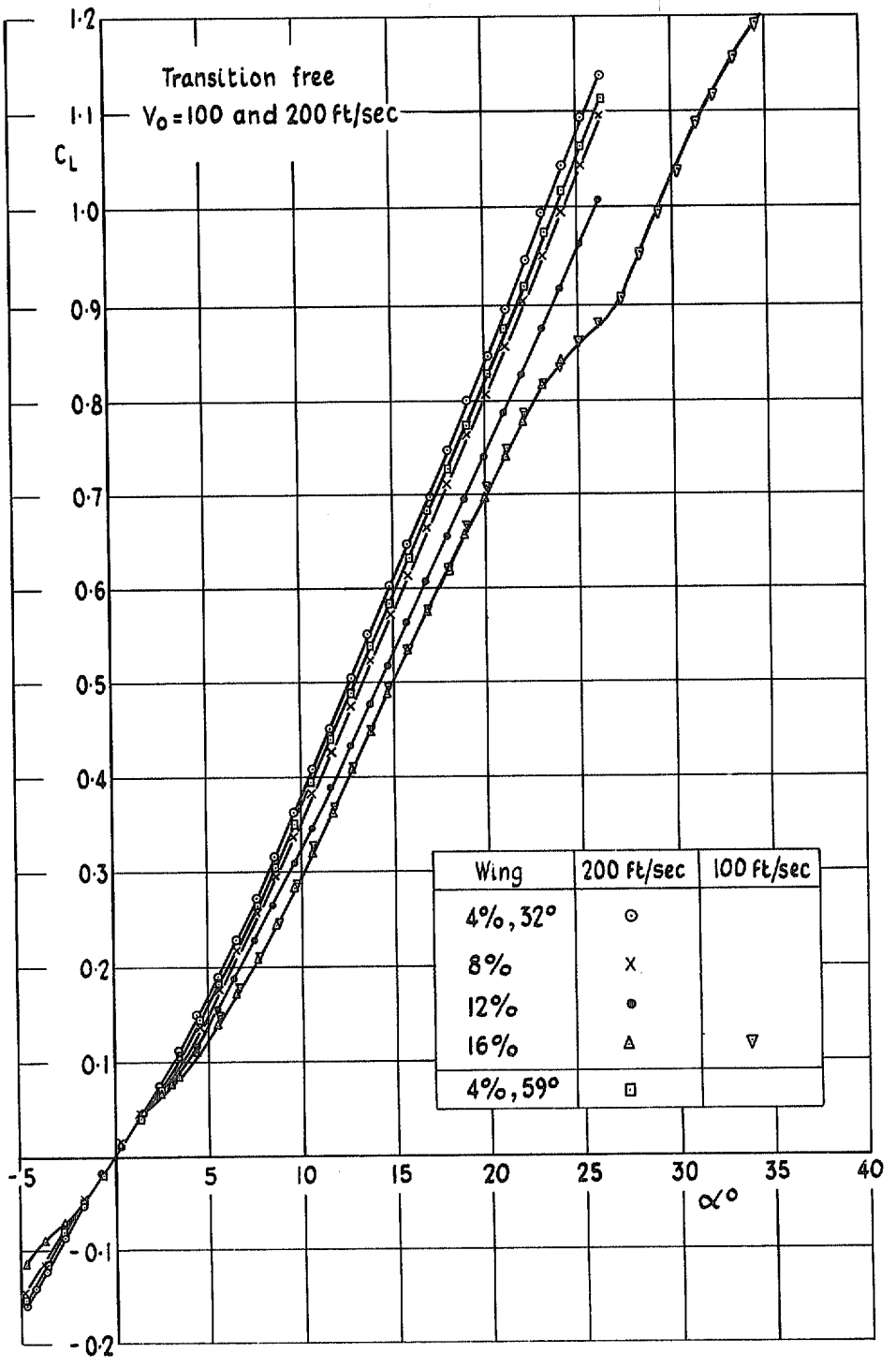

FIG. 3. Effect of thickness on lift.

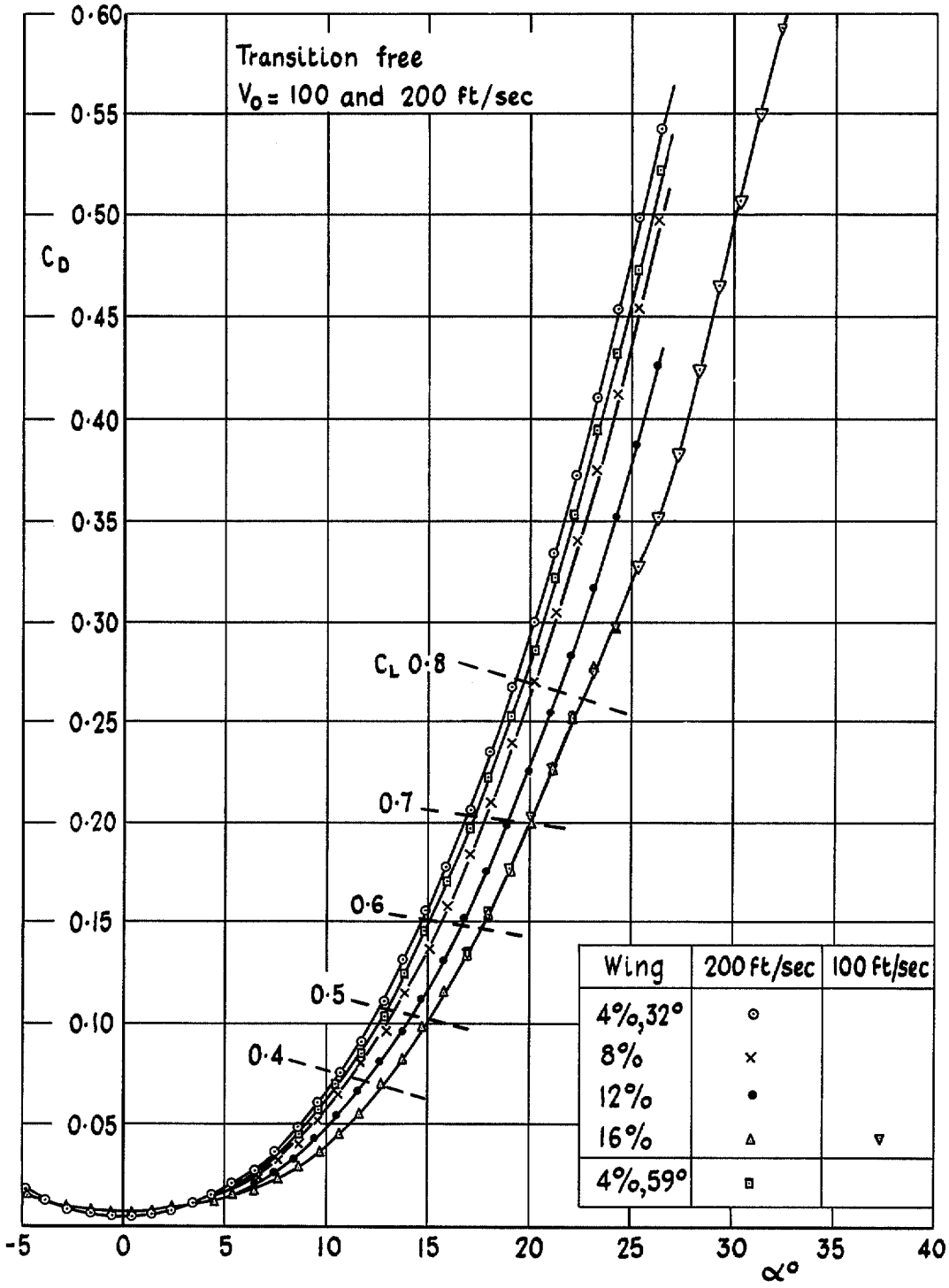

FIG. 4. Effect of thickness on drag.

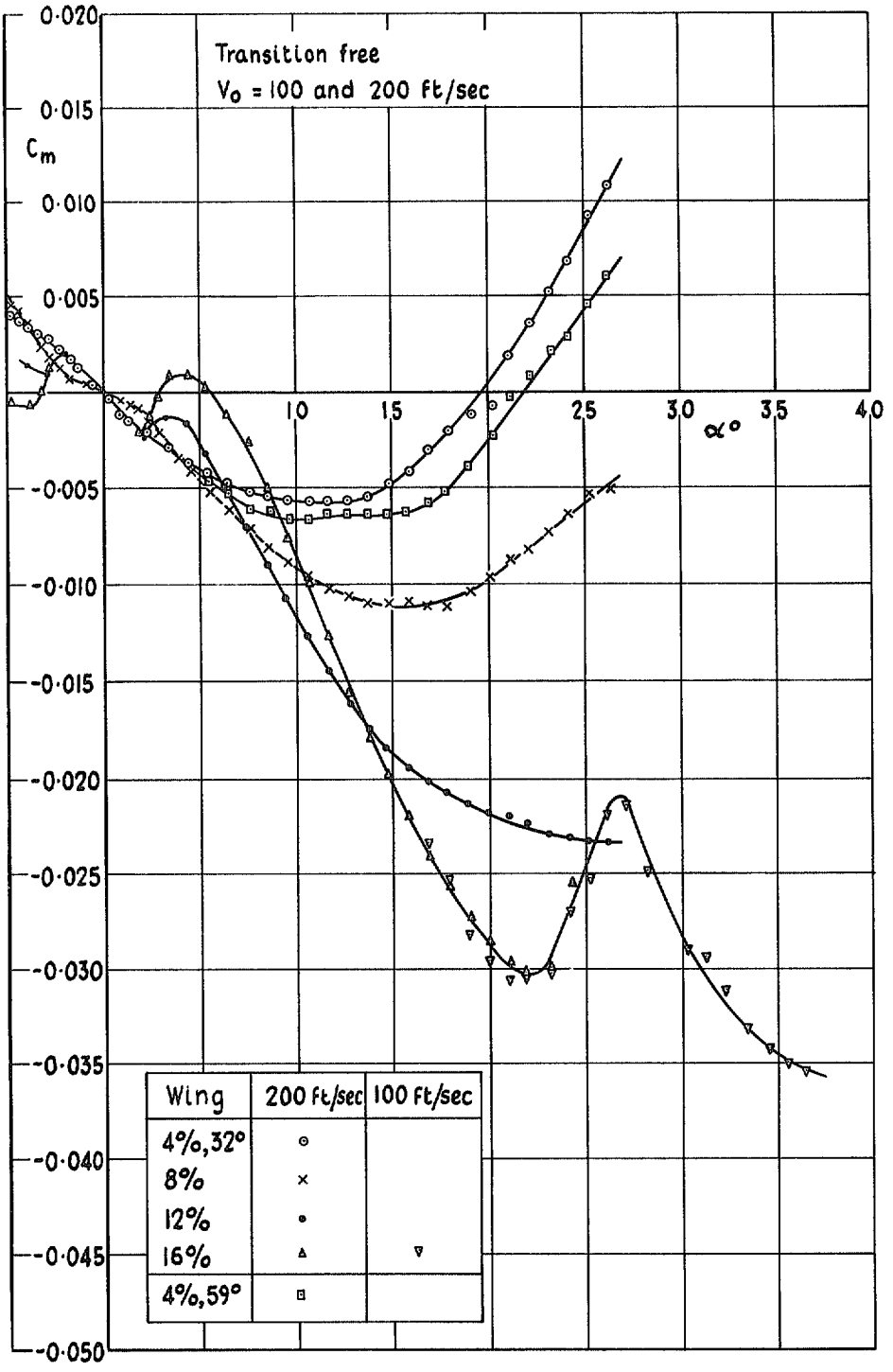

FIG. 5. Effect of thickness on pitching moment.

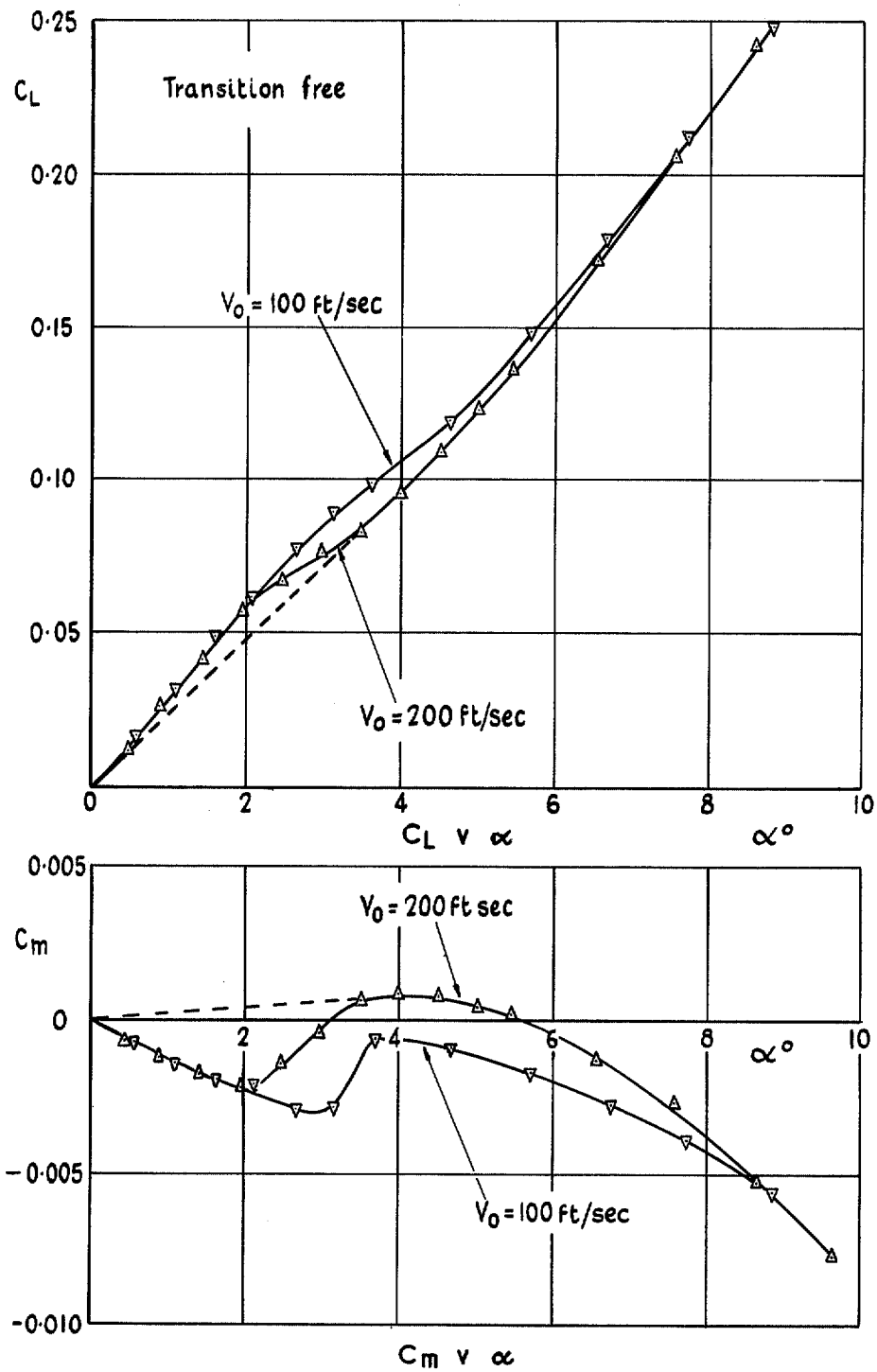

FIG. 6. Effect of Reynolds number on lift and pitching moment of 16% wing at low incidence.

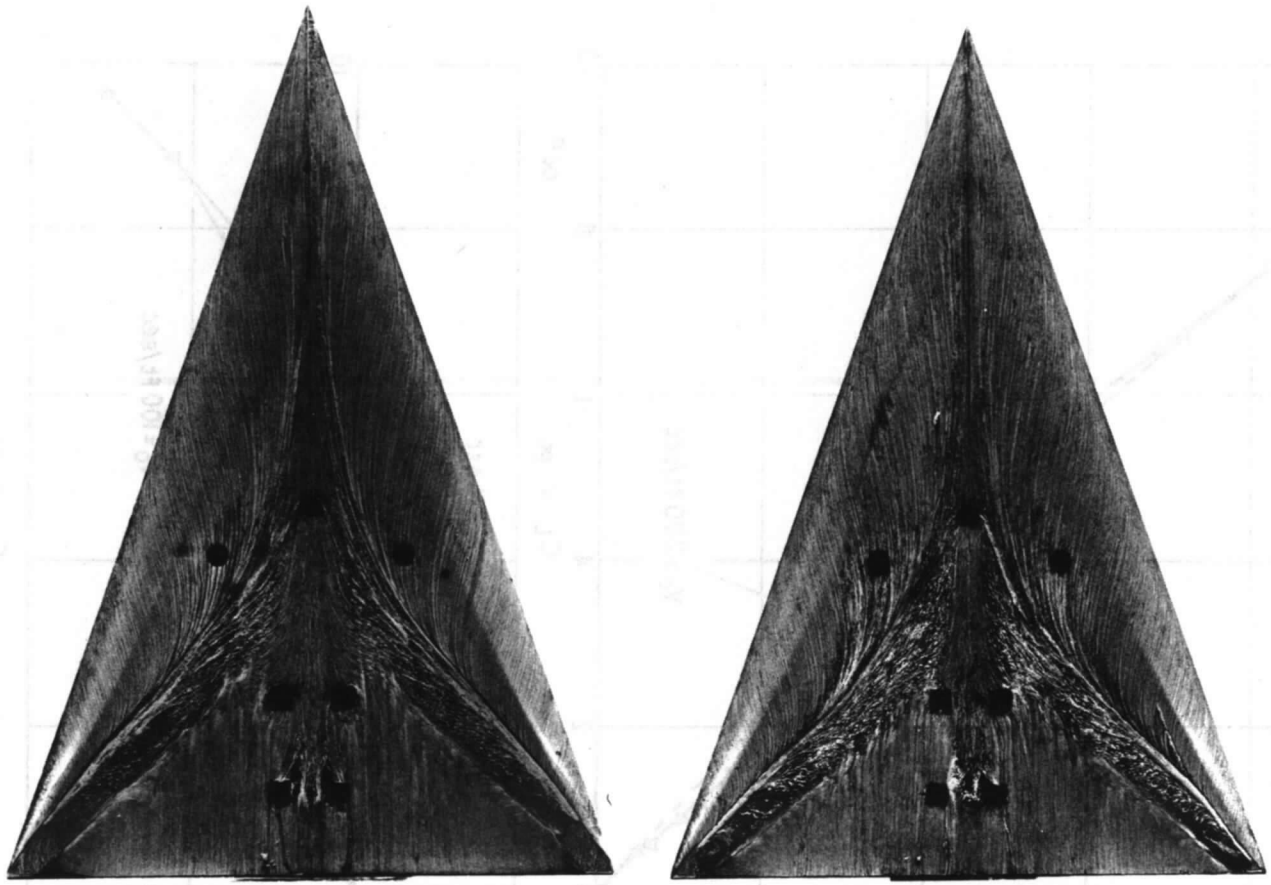

a. Upper surface

b. Lower surface

FIG. 7. Surface flow patterns at $\alpha = 1{\cdot}5°$ $V_o = 100$ ft/sec.

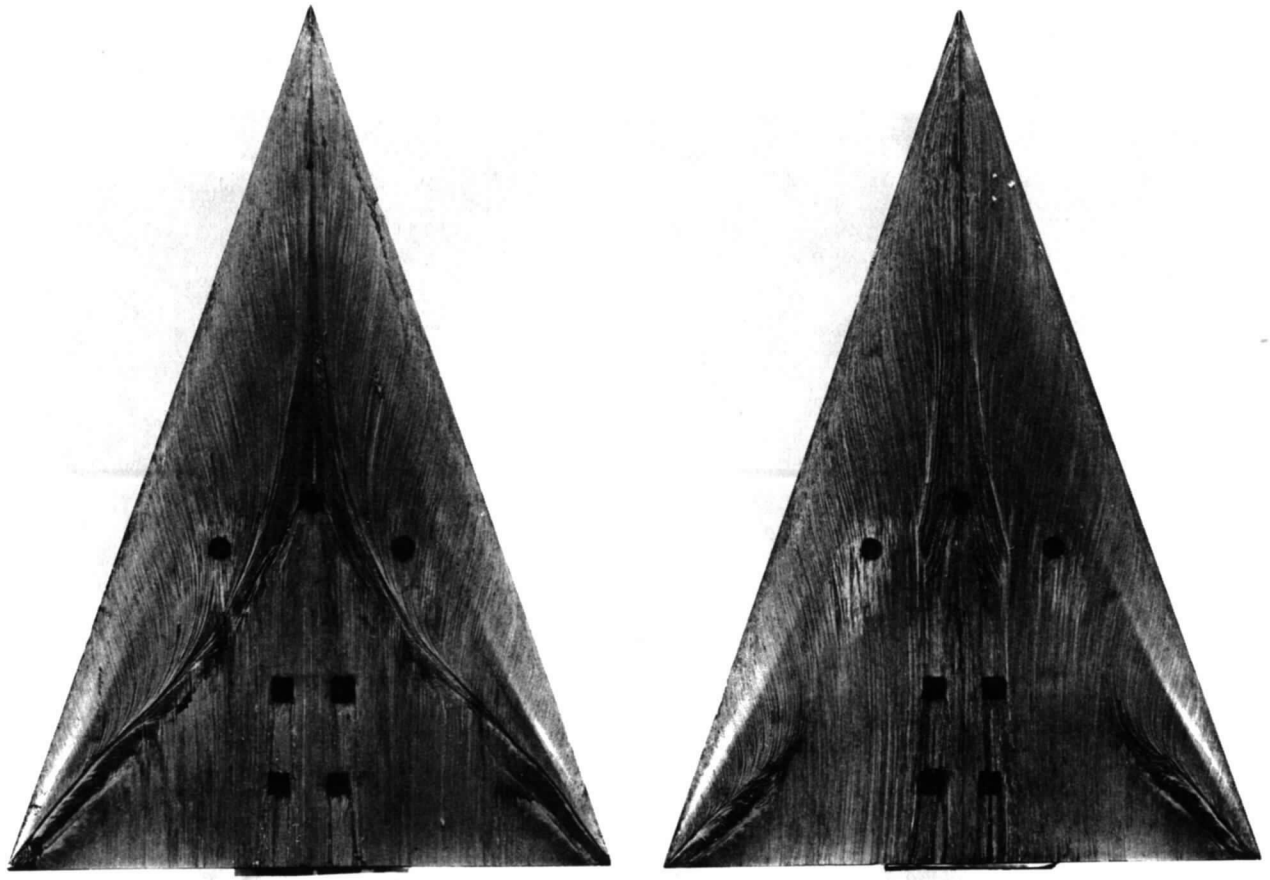

a. Upper surface

b. Lower surface

FIG. 8. Surface flow patterns at $\alpha = 1{\cdot}5°$ $V_o = 200$ ft/sec.

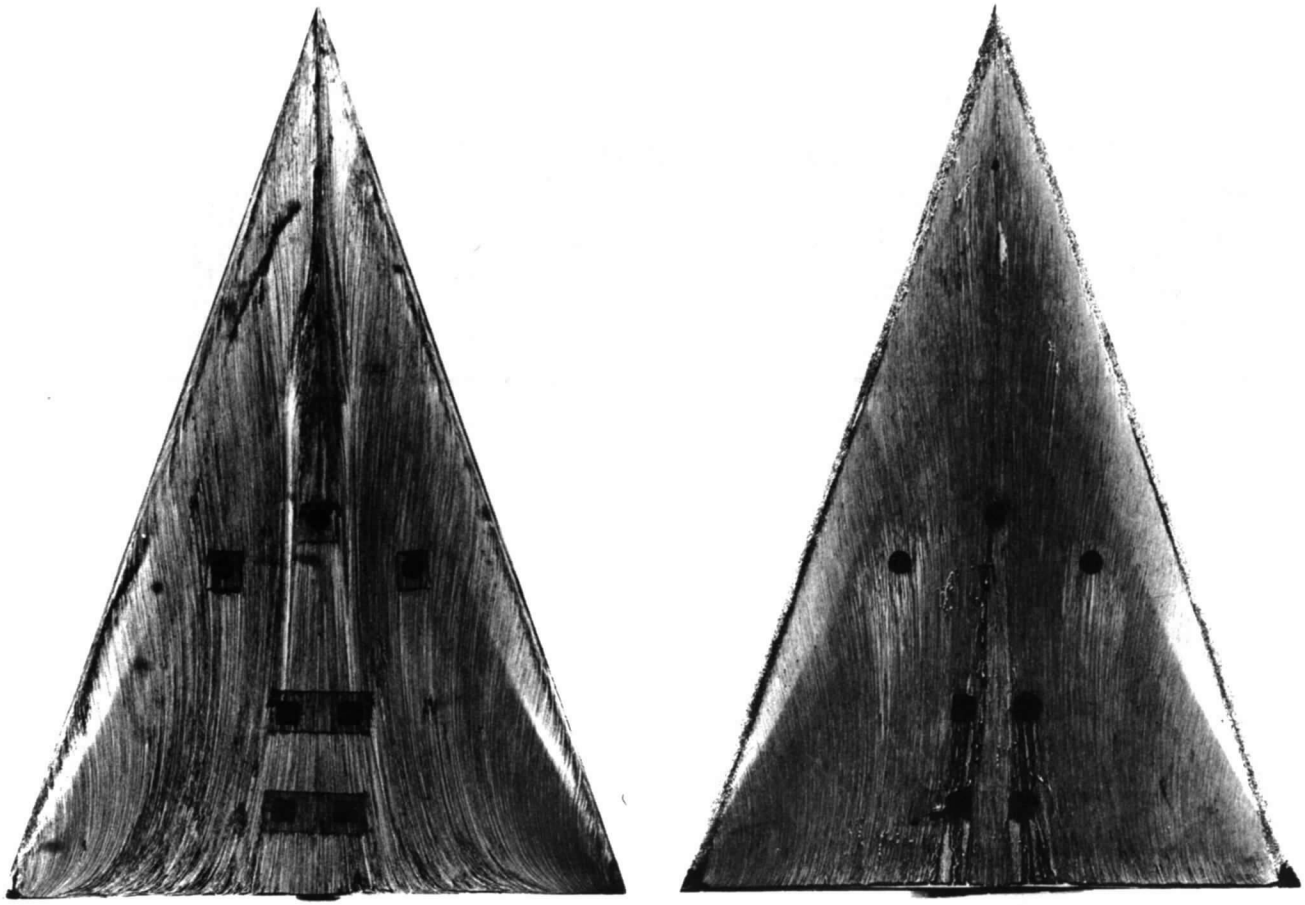

a. Upper surface, $\alpha = 5°$

b. Upper surface with roughness, $\alpha = 1{\cdot}5°$.

FIG. 9. Surface flow patterns at $V_o = 100$ ft/sec.

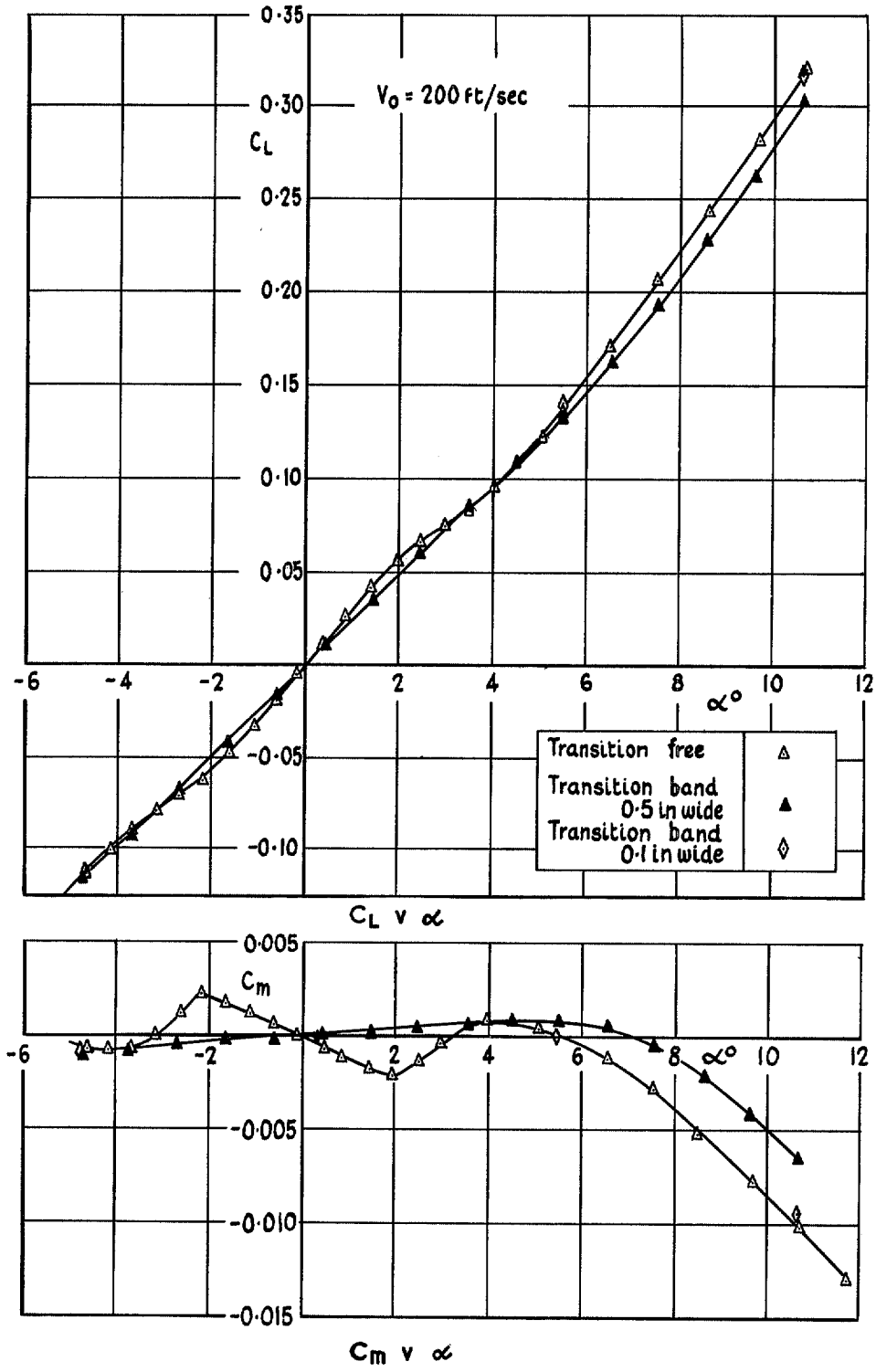

FIG. 10. Effect of roughness on lift and pitching moment of 16⩾ wing at low incidence.

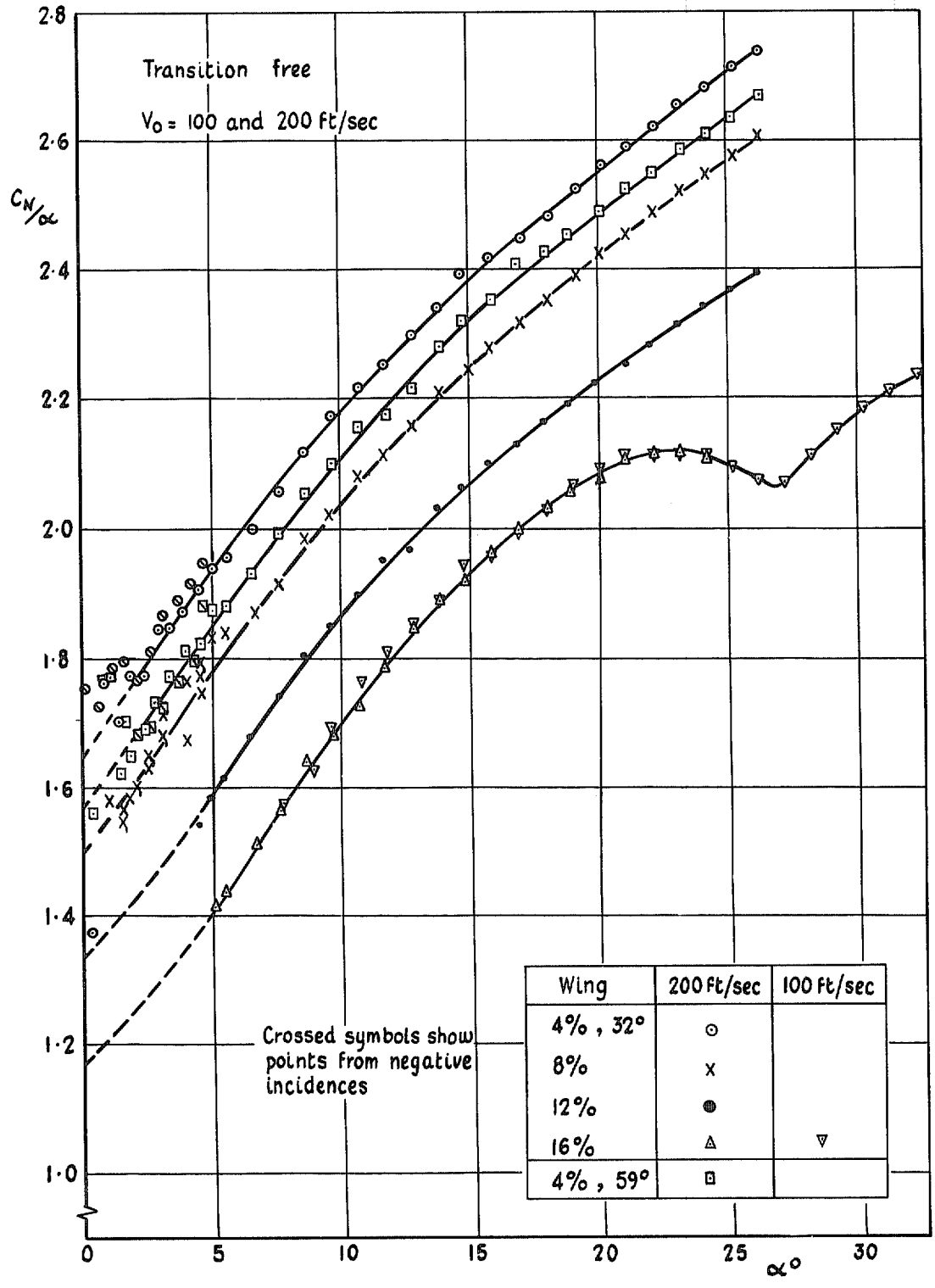

FIG. 11. Effect of thickness on C_N/α.

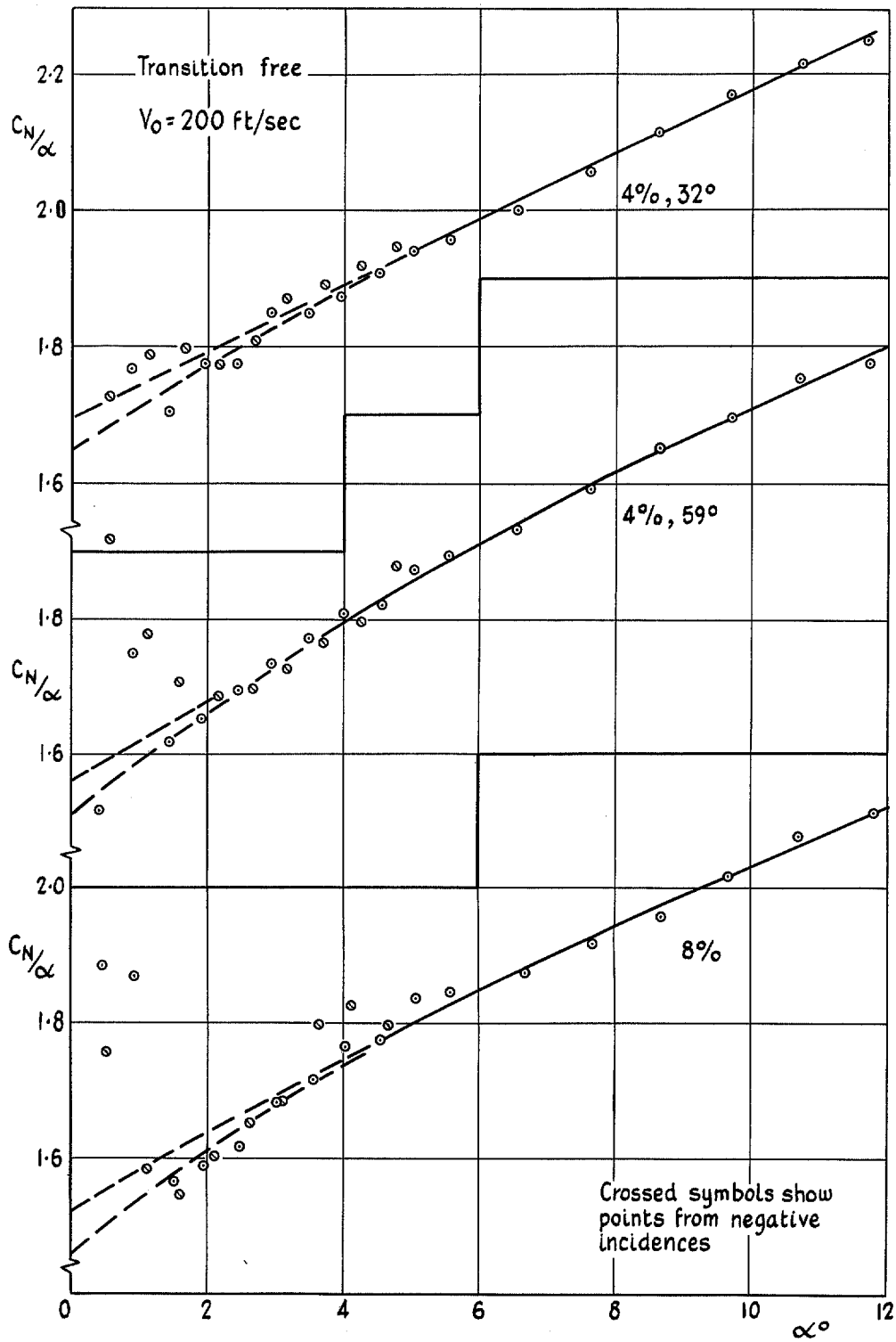

FIG. 12. C_N/α at low incidence for 4% and 8% wings.

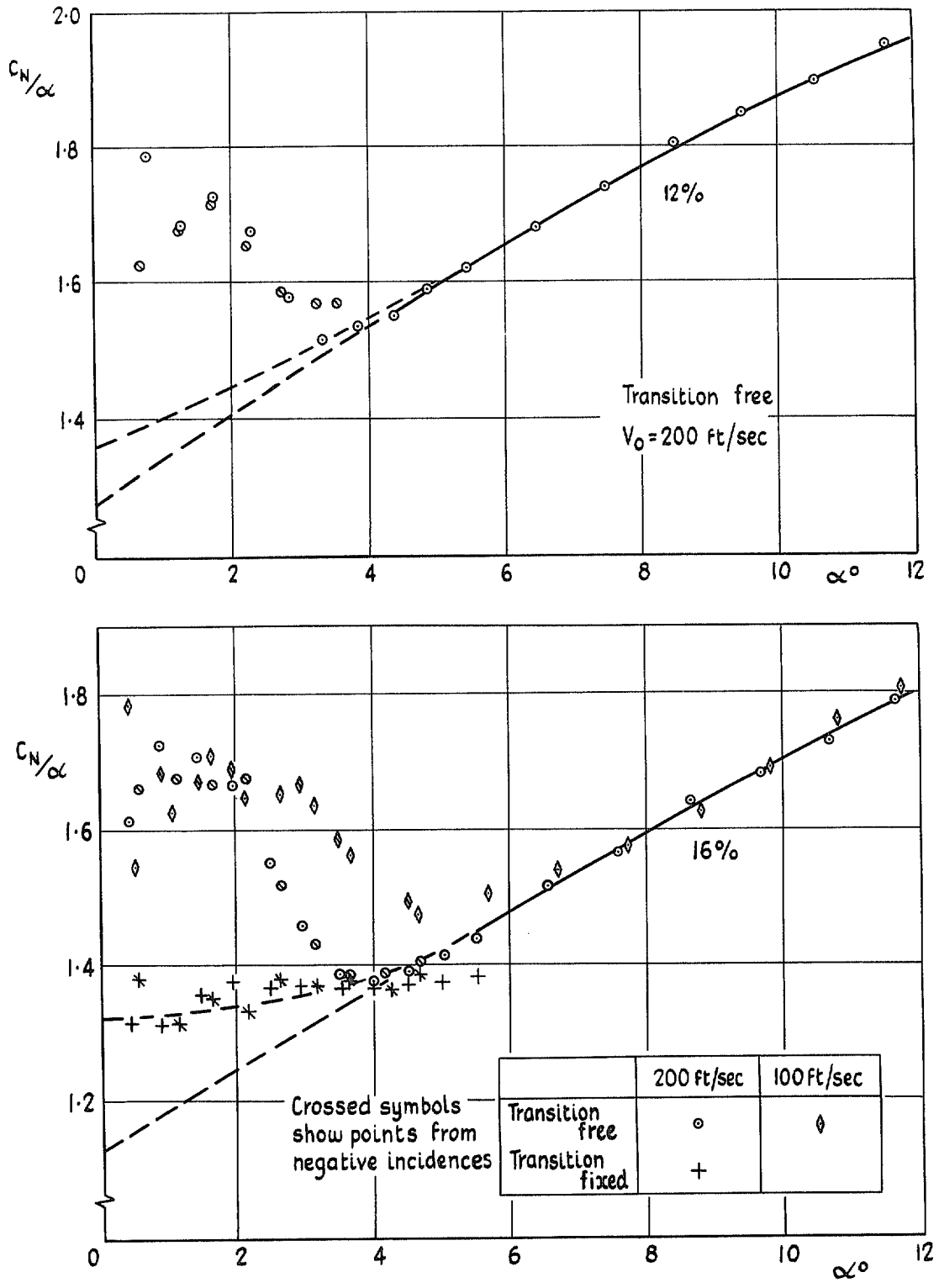

FIG. 13. C_N/α at low incidence for 12% and 16% wings.

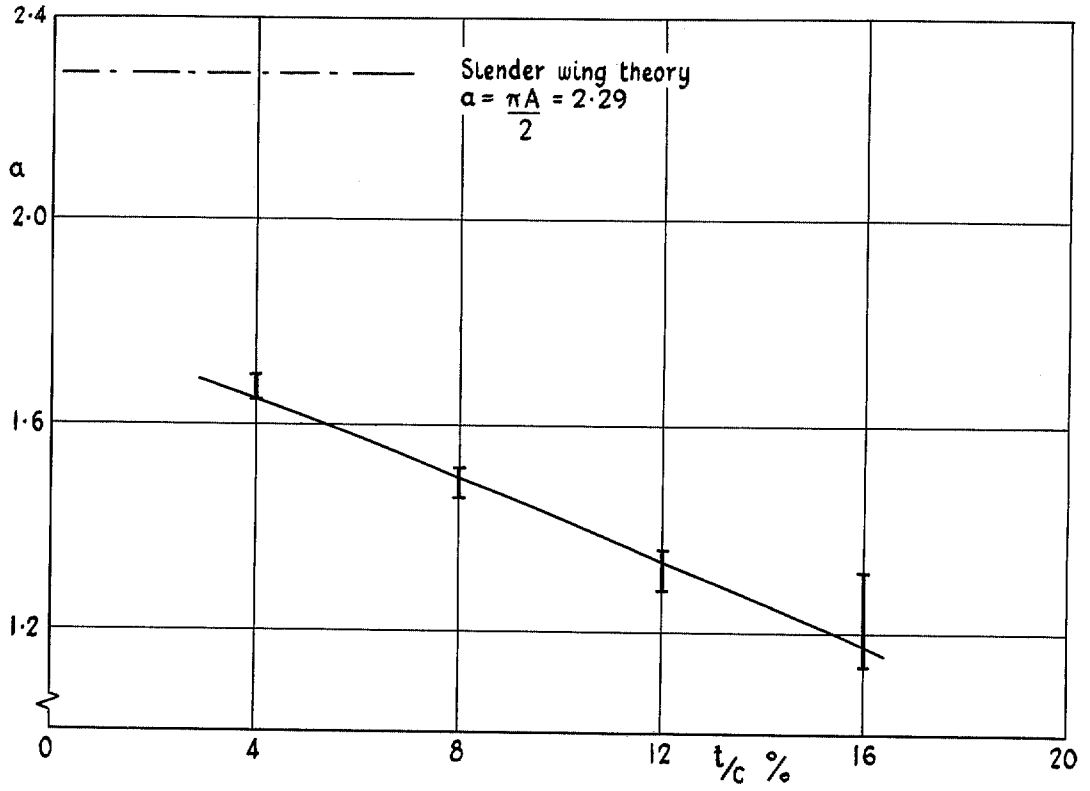

FIG. 14. Variation of a with thickness.

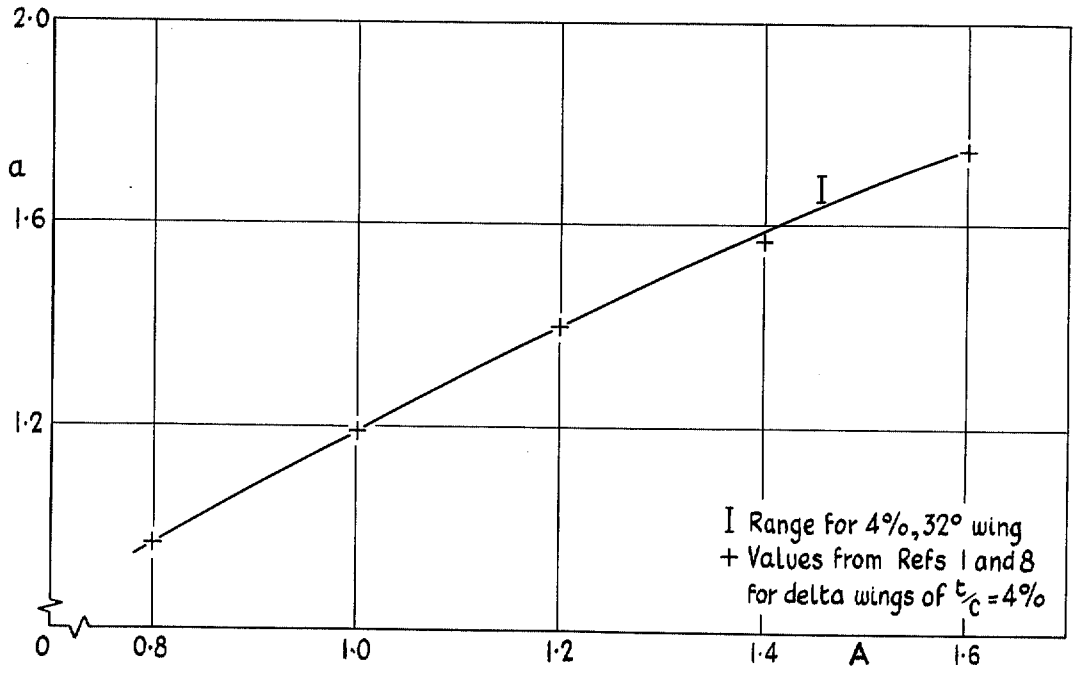

FIG. 15. Variation of a with aspect ratio for delta wings.

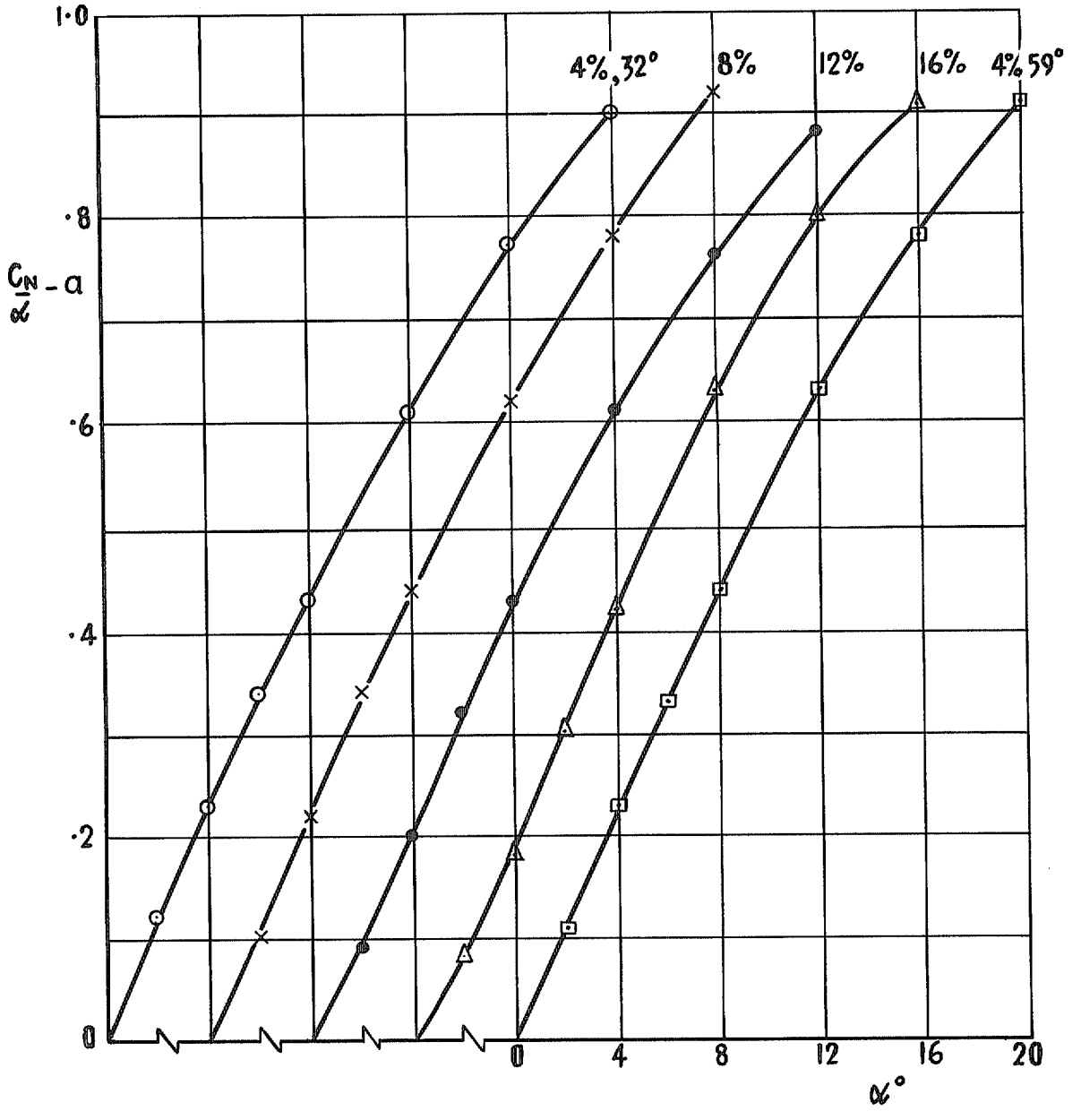

FIG. 16. Effect of thickness on the non-linear component of normal force.

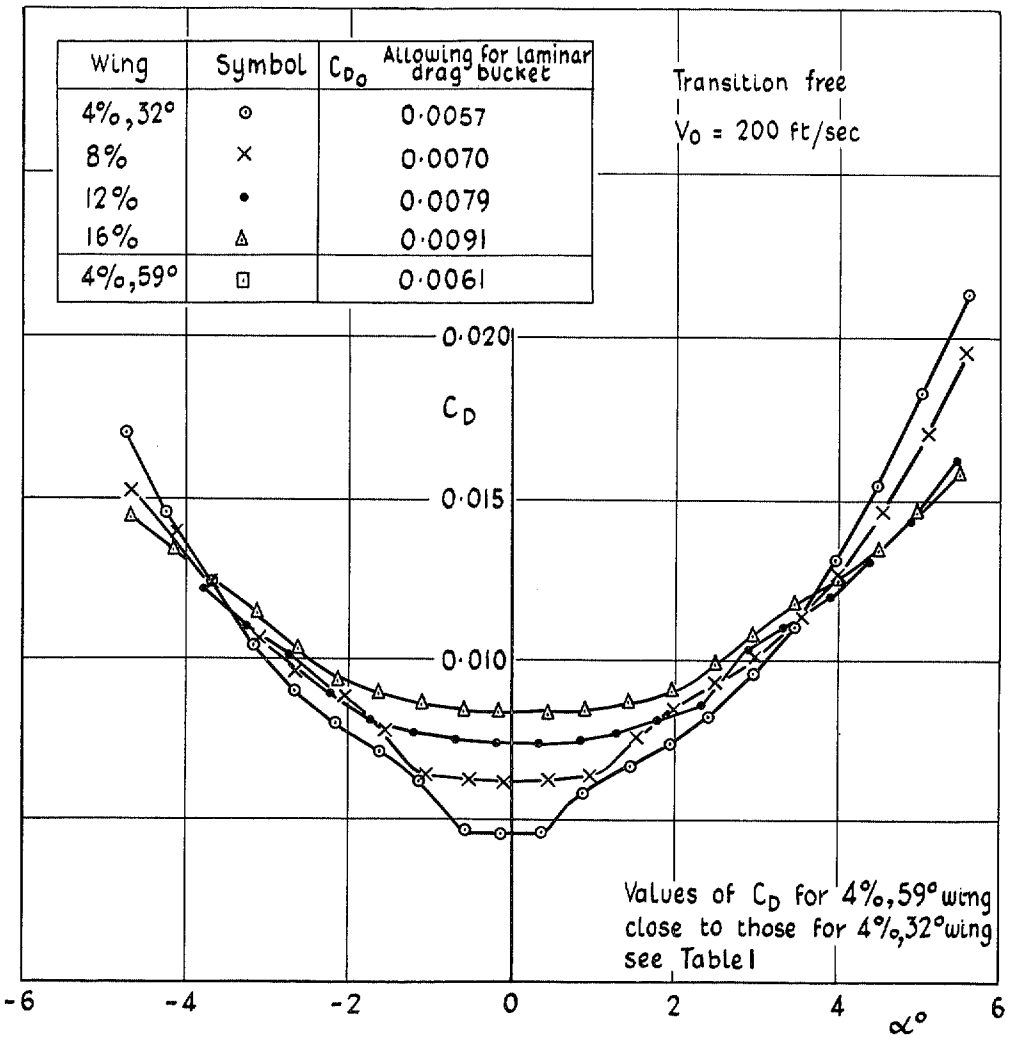

FIG. 17. Effect of thickness on drag at low incidence.

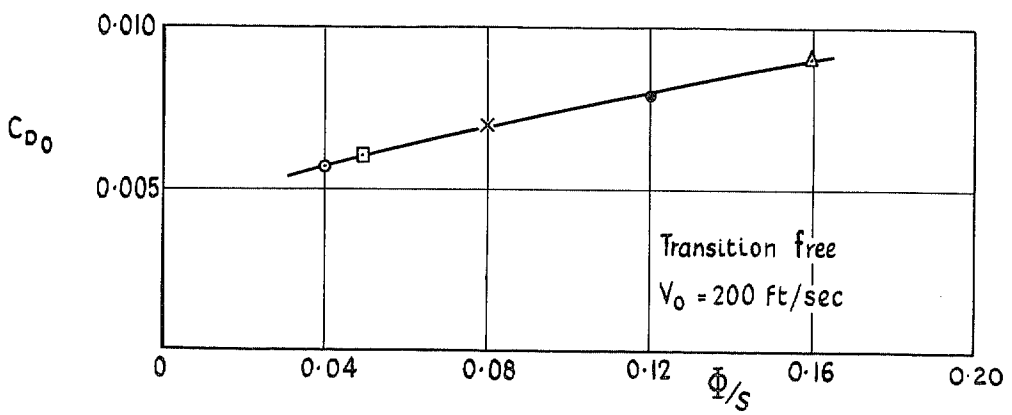

FIG. 18. Variation of corrected C_{D_0} with thickness parameter.

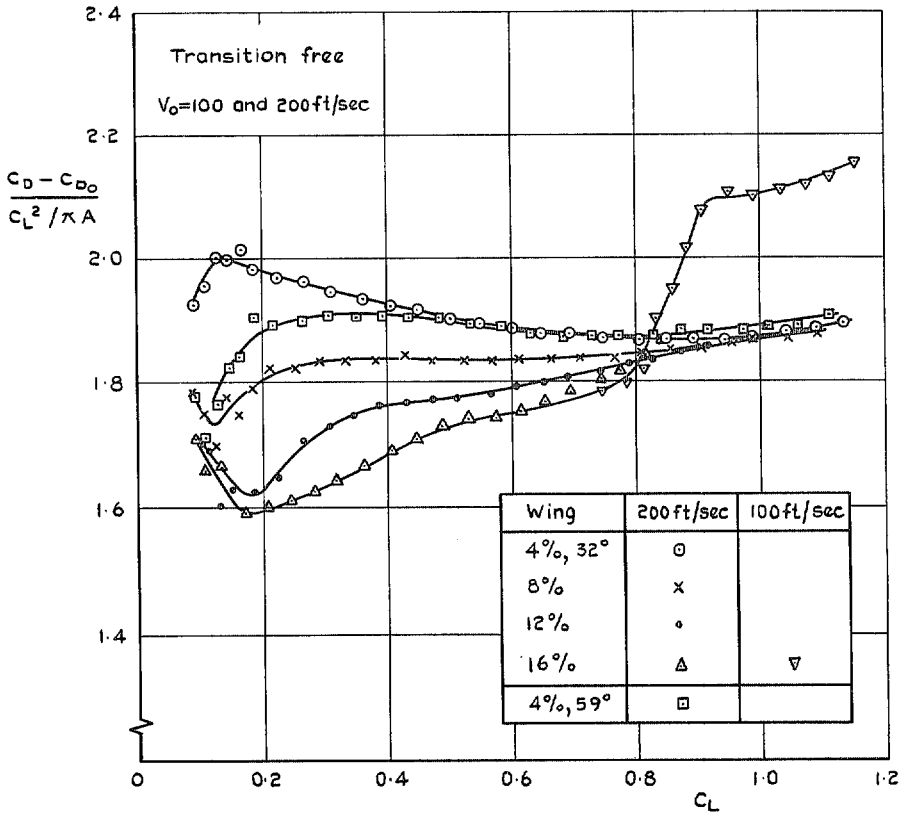

FIG. 19. Effect of thickness on lift-dependent drag factor.

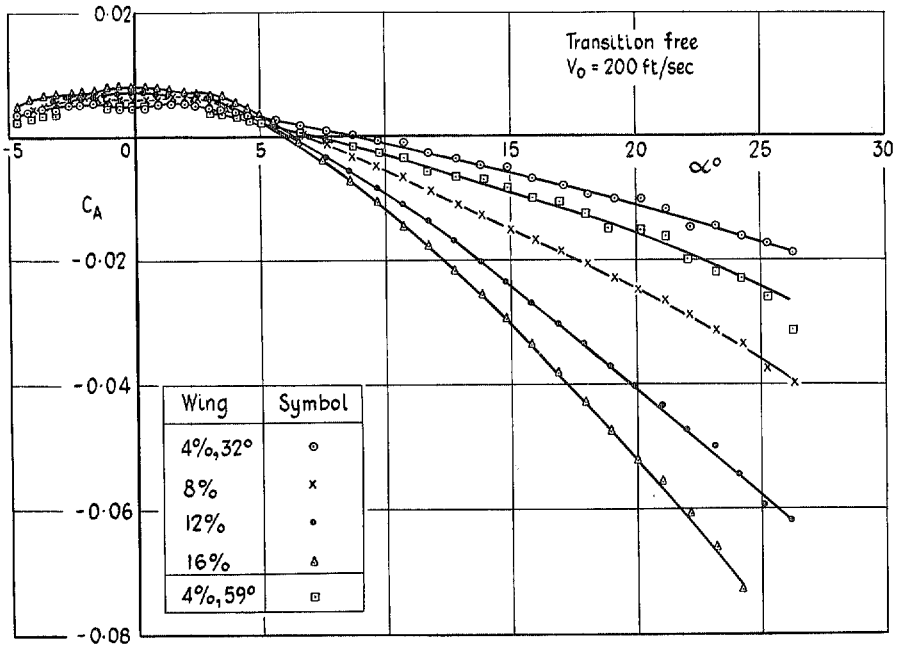

FIG. 20. Effect of thickness on axial force coefficient.

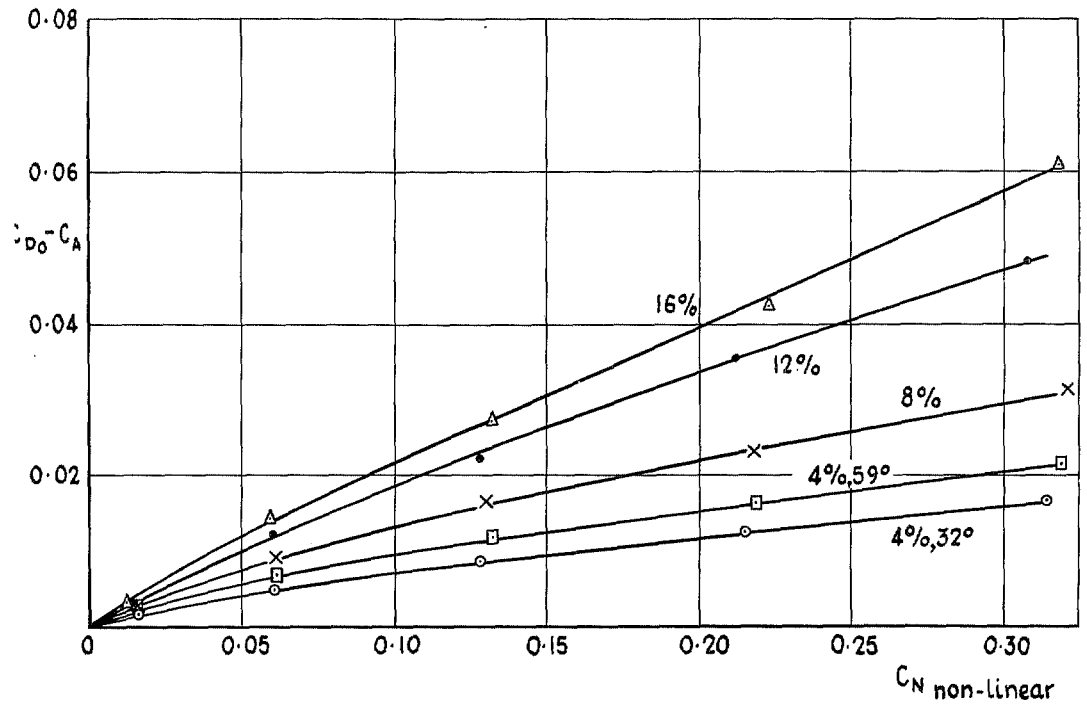

FIG. 21. Effect of thickness on thrust component due to leading-edge vortices.

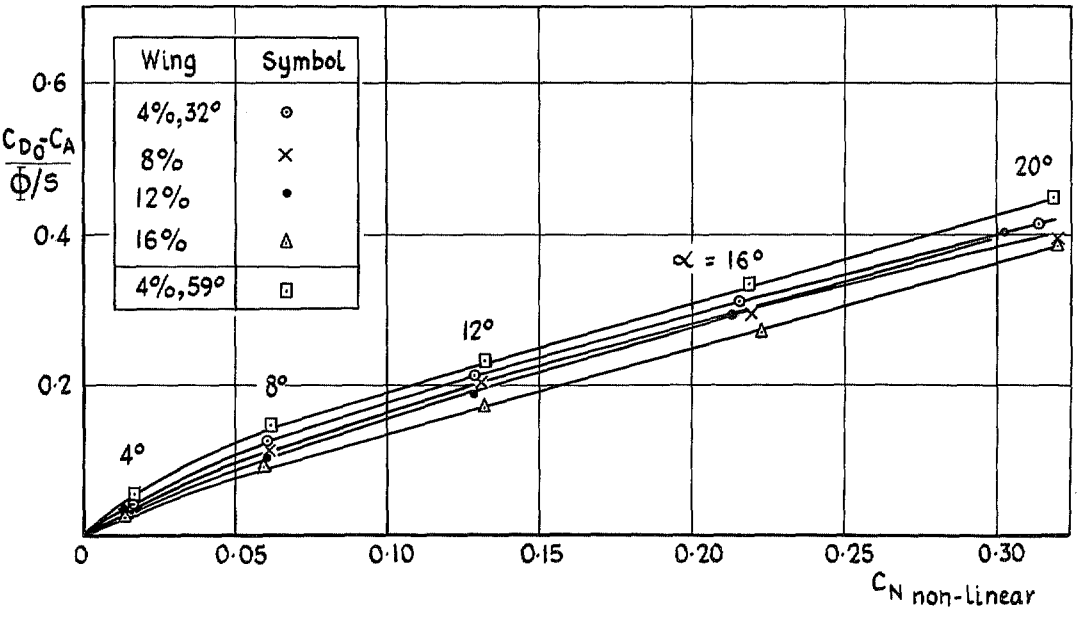

FIG. 22. Thrust component referred to frontal area.

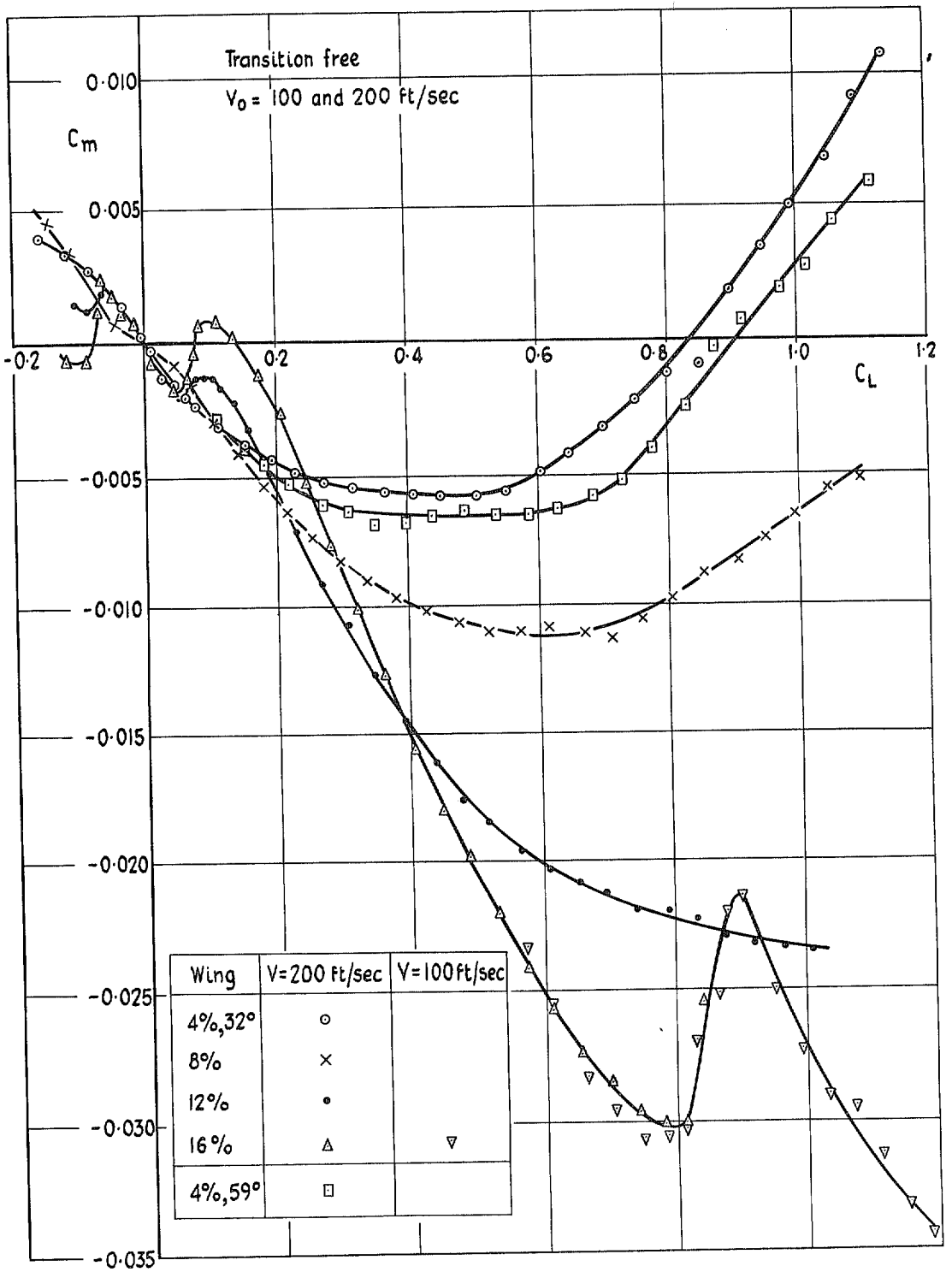

FIG. 23. Effect of thickness on the variation of pitching moment with lift.

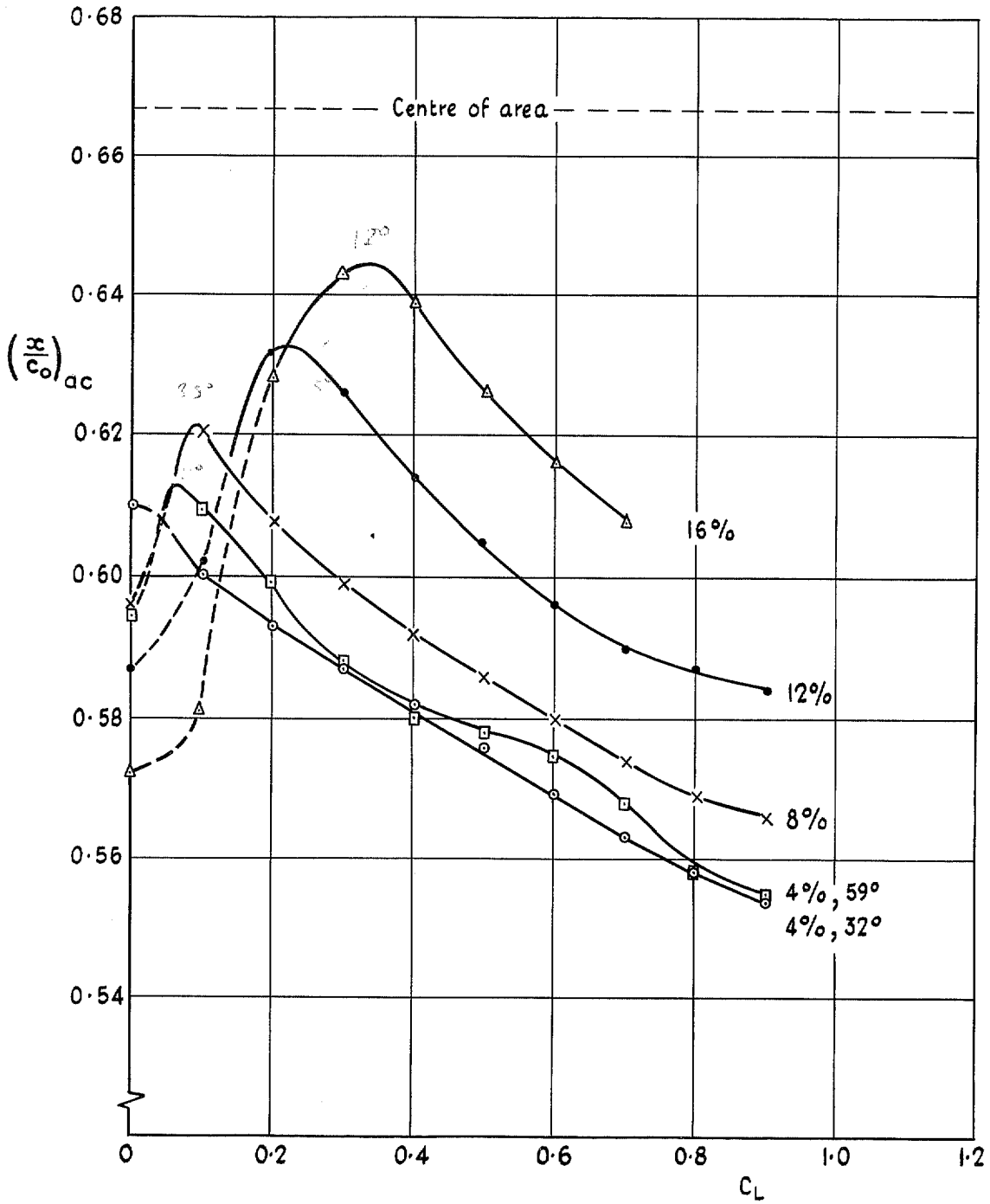

FIG. 24. Effect of thickness on the position of the aerodynamic centre.

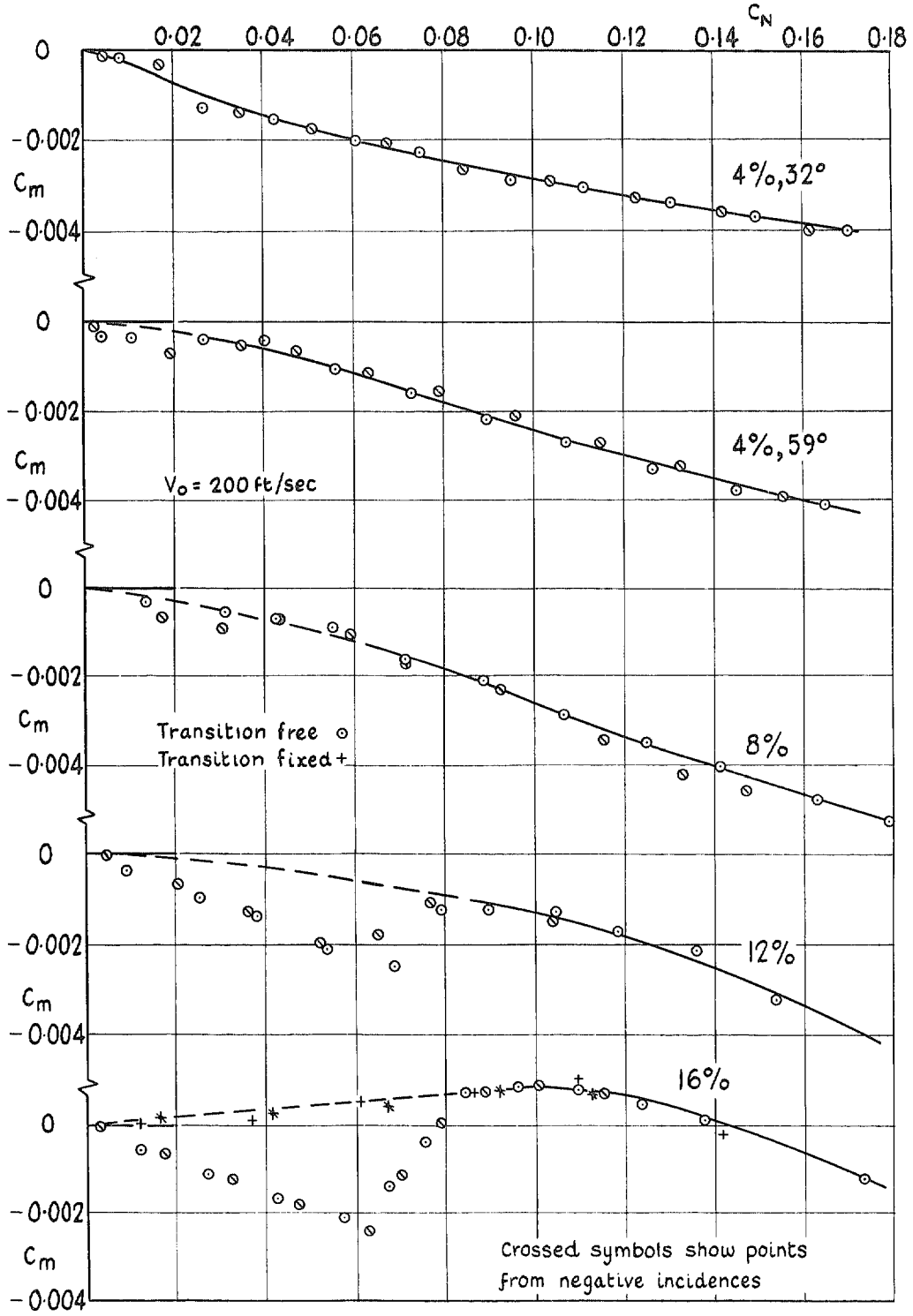

FIG. 25. C_m v C_N at low incidence.

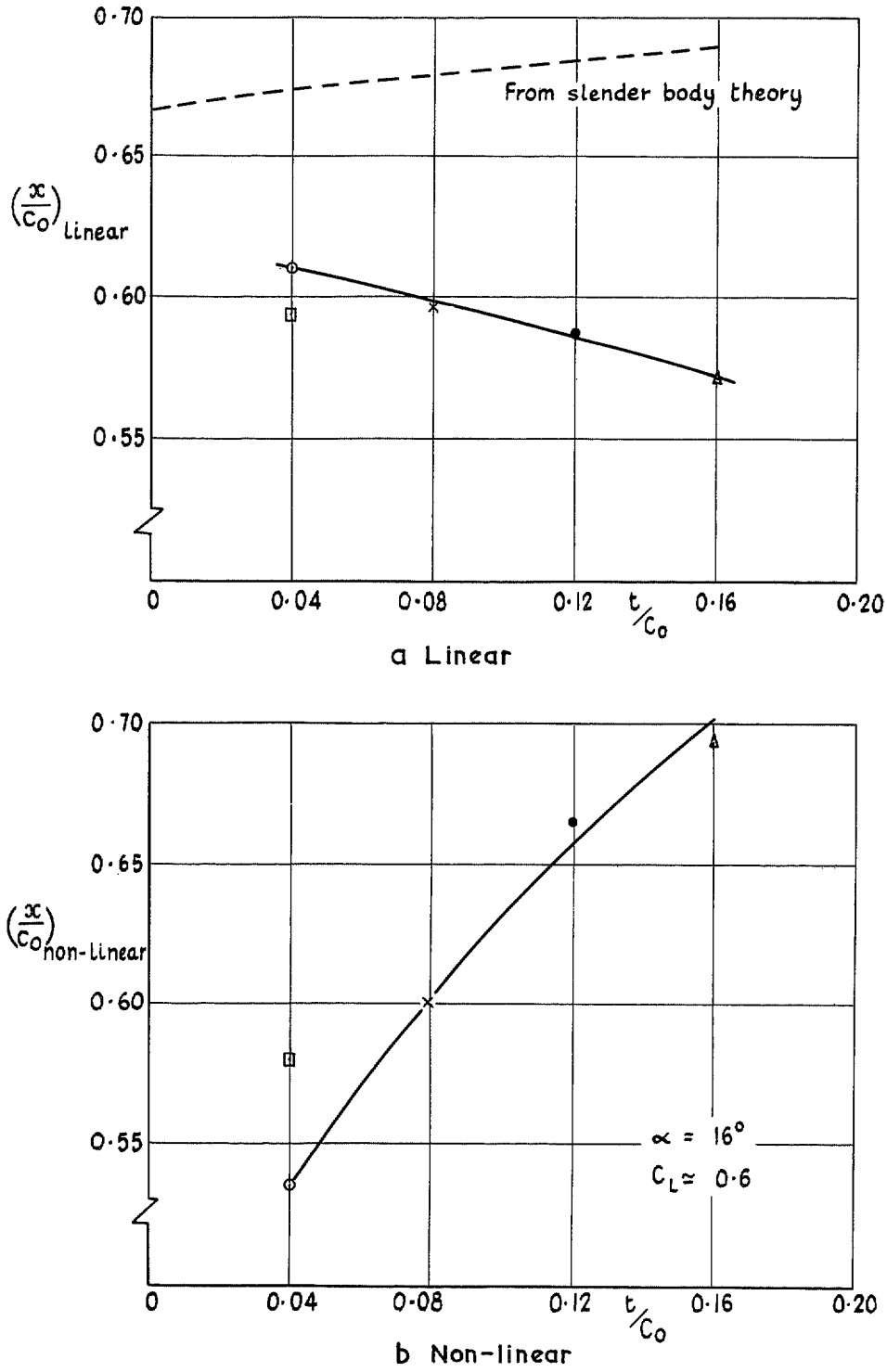

FIG. 26. Effect of thickness on the points of action of the linear and non-linear force components.

Printed in Wales for Her Majesty's Stationery Office by Allens Printers (Wales) Limited.
Dd. 502110 K.5.

Published by
HER MAJESTY'S STATIONERY OFFICE

To be purchased from
49 High Holborn, London WC1V 6HB
13a Castle Street, Edinburgh EH2 3AR
109 St Mary Street, Cardiff CF1 1JW
Brazennose Street, Manchester M60 8AS
50 Fairfax Street, Bristol BS1 3DE
258 Broad Street, Birmingham B1 2HE
80 Chichester Street, Belfast BT1 4JY
or through booksellers

R. & M. No. 3673
SBN 11 470413 9